A high-velocity narrow absorption line outflow in the quasar J212329.46 − 005052.9

F. Hamann,[1]★ N. Kanekar,[2] J. X. Prochaska,[3,4] M. T. Murphy,[5] S. Ellison,[6] A. L. Malec,[5] N. Milutinovic[6] and W. Ubachs[7]

[1]*Department of Astronomy, University of Florida, Gainesville, FL 32611-2055, USA*
[2]*Ramanujan Fellow, National Centre for Radio Astrophysics, Tata Institute of Fundamental Research, Ganeshkhind, Pune 411007, India*
[3]*Department of Astronomy and Astrophysics, University of California, Santa Cruz, Santa Cruz, CA 95064, USA*
[4]*University of California Observatories – Lick Observatory, University of California, Santa Cruz, CA 95064, USA*
[5]*Centre for Astrophysics & Supercomputing, Swinburne University of Technology, Melbourne, Victoria 3122, Australia*
[6]*Department of Physics & Astronomy, University of Victoria, Victoria, BC, V8P 1A1, Canada*
[7]*Laser Centre, VU University, De Boelelaan 1081, 1081 HV Amsterdam, the Netherlands*

ABSTRACT

We report on the discovery of a high-velocity narrow absorption line outflow in the redshift 2.3 quasar J212329.46 − 005052.9. Five distinct outflow systems are detected with velocity shifts from −9710 to −14 050 km s^{-1} and C IV λλ1548, 1551 linewidths of FWHM ≈ 62–164 km s^{-1}. This outflow is remarkable for having high speeds and a degree of ionization similar to broad absorption line (BAL) flows, but linewidths roughly 100 times narrower than BALs and no apparent X-ray absorption. This is also, to our knowledge, the highest-velocity narrow absorption line system confirmed to be in a quasar outflow by all three indicators of line variability, smooth superthermal line profiles and doublet ratios that require partial covering of the quasar continuum source. All five systems have stronger absorption in O VI λλ1032, 1038 than C IV with no lower ionization metal lines detected. Their line variabilities also appear coordinated, with each system showing larger changes in C IV than O VI and line strength variations accompanied by nearly commensurate changes in the absorber covering fractions. The metallicity is approximately twice solar.

These data require five distinct outflow structures with similar kinematics, physical conditions and characteristic sizes of order 0.01–0.02 pc (based on partial covering). The coordinated line variations, occurring on time-scales ≤0.63 yr (quasar frame), are best explained by global changes in the outflow ionization caused by changes in the quasar's ionizing flux. An upper limit on the acceleration, ≲3 km s^{-1} yr^{-1}, is consistent with blobs of gas that are gravitationally unbound and coasting freely ≳5 pc from the central black hole. Additional constraints from the variability time indicate that the full range of plausible distances is $5 \lesssim R \lesssim 1100$ pc. However, if these small absorbing structures were created in the inner flow, they should be near the ∼5 pc minimum radius because they can travel just a few pc before dissipating (without external confinement). An apparent double line-lock in C IV suggests that the flow was radiatively accelerated and its present trajectory is within ∼16° of the radial (line-of-sight) direction. The absence of strong X-ray absorption shows that radiative shielding in the far-UV and X-rays is not needed to maintain moderate BAL-like ionizations and therefore, apparently, it is not needed to facilitate the radiative acceleration to high speeds. We argue that the ionization is moderated, instead, by high gas densities in small outflow substructures. Finally, we estimate that the kinetic energy yield from this outflow is at least 2 orders of magnitude too low to be important for feedback to the host galaxy's evolution.

Key words: galaxies: active – quasars: absorption lines – quasars: general – quasars: individual: J212329.46 − 005052.9.

★E-mail: hamann@astro.ufl.edu

1 INTRODUCTION

High-velocity outflows from quasars appear to be a natural part of the accretion process. They are detected most conspicuously via broad absorption lines (BALs) in quasar spectra, with velocity widths >2000 km s^{-1} (by definition; Weymann et al. 1991) and flow speeds from a few thousand to roughly $10\,000$–$30\,000$ km s^{-1} (see also Korista et al. 1993; Trump et al. 2006). However, quasar outflows can also produce narrow absorption lines (NALs), with velocity widths less than a few hundred km s^{-1}, as well as mini-BALs, which are loosely defined as intermediate between NALs and BALs (e.g. Hamann & Sabra 2004; Nestor, Hamann & Rodriguez Hidalgo 2008; Rodríguez Hidalgo et al., in preparation). These narrower outflow lines are more common than BALs (Richards 2001; Misawa et al. 2007a; Nestor et al. 2008; Wild et al. 2008; Gibson et al. 2009a; Rodríguez Hidalgo et al., in preparation). Overall, it is estimated that >50 per cent of optically selected quasars have at least one type of outflow absorption line in their rest-frame UV spectra (Ganguly & Brotherton 2008; Rodríguez Hidalgo et al., in preparation). The flows themselves are probably present in all quasars if, as expected, the outflowing gas covers just a fraction of the sky as seen from the central emission source (e.g. Hamann, Korista & Morris 1993).

Quasar outflows have gained attention recently as a mechanism that can physically couple quasars to the evolution of their host galaxies. In particular, some models of galaxy evolution invoke the kinetic energy 'feedback' from an accreting supermassive black hole (SMBH) to regulate both the star formation in the host galaxies and the infall of matter towards the central SMBH (Kauffmann & Haehnelt 2000; Granato et al. 2004; Di Matteo, Springel & Hernquist 2005; Hopkins & Elvis 2010, and references therein). This type of coupling via feedback could provide a natural explanation for the observed mass correlation between SMBHs and their host galaxy spheroids (Tremaine et al. 2002; Marconi & Hunt 2003; Häring & Rix 2004). The kinetic energy luminosity, L_K, needed for significant feedback from a quasar outflow is believed to be just a few per cent of the quasar bolometric (photon) luminosity, e.g. $L_K/L \sim 5$ per cent (Scannapieco & Oh 2004; Di Matteo et al. 2005; Prochaska & Hennawi 2009).

Unfortunately, many aspects of the energetics and physical properties of quasar outflows remain poorly understood. Computational models aimed mainly at BALs attribute the flows to gas lifted off the accretion disc and driven outward to high speeds by radiation pressure or magneto-centrifugal forces (Murray et al. 1995; Murray & Chiang 1997; Proga & Kallman 2004; Everett 2005). Radiative forces are expected to dominate in quasars, where the bolometric luminosities are a substantial fraction of the Eddington luminosity (Everett 2005).

One essential requirement for radiative driving is that the outflow is not too highly ionized, so it can maintain significant line and bound-free continuum opacities across the main acceleration region. This is not trivial for flows launched from the inner accretion disc, near the quasar's intense source of ionizing radiation. Murray et al. (1995) proposed that the outflow ionization is moderated by a high column density of roughly stationary material that serves as a radiative shield at the base of the flow (also Murray & Chiang 1997). The shielding medium is itself too ionized and too transparent to be driven radiatively to high speeds, but it might have enough continuous opacity in the far-UV and X-rays to lower the ionization and thereby facilitate the acceleration of the gas directly behind it (i.e. farther from the emission source). This scenario is supported by observations showing that BAL quasars are heavily obscured in

X-rays, consistent with strong radiative shielding (Green & Mathur 1996; Mathur et al. 2000; Gallagher et al. 2002, 2006). However, other observations indicate that quasars with NAL or mini-BAL outflows have substantially less X-ray absorption (Misawa et al. 2008; Chartas et al. 2009; Gibson et al. 2009b). This disparity in the X-ray results, between BALs on the one hand and NALs and mini-BALs on the other, presents an important challenge to the paradigm of radiative acceleration behind an X-ray/far-UV shield (see also Section 4.5 below).

A central problem is our poor understanding of the physical relationships between BAL, NAL and mini-BAL outflows. One possibility is that the different line types are simply different manifestations of a single outflow phenomenon viewed at different angles. For example, it is often supposed that BALs form in the main body of the outflow near the accretion disc plane, while NALs and mini-BALs form along sightlines that skim the edges of the BAL flow at higher latitudes above the disc (Ganguly et al. 2001; Chartas et al. 2009). There could also be evolutionary effects. For example, NALs and mini-BALs might represent the tentative beginning or end stages of a more powerful BAL outflow phase (Hamann et al. 2008). There is some evidence for outflow evolution in that a particular variety of low-ionization BALs (the so-called FeLoBALs) is found preferentially in dusty young host galaxies with high star formation rates (Farrah et al. 2007). Variability studies have shown further that BALs and mini-BALs in quasar spectra can appear, disappear or swap identities (where a BAL becomes a mini-BAL or vice versa) on time-scales of months to years in the quasar rest frame (Gibson et al. 2008, 2010; Hamann et al. 2008; Leighly et al. 2009; Capellupo et al. 2010; Rodríguez Hidalgo et al., in preparation). The true relationship between outflow NALs, BALs and mini-BALs probably involves an amalgam of orientation and time-dependent effects.

To build a more complete picture of quasar outflows, we need better observational constraints on the physical properties of each outflow type. NAL outflows present a unique challenge because they are difficult to identify. Most narrow absorption lines in quasar spectra form in cosmologically intervening gas that has no relationship to the background quasar. Statistical studies that examine the velocity distributions of the narrow metal lines (Nestor et al. 2008; Wild et al. 2008), or correlations between the incidence of these lines and the properties of the background quasars (Richards 2001), indicate that significant fractions of the narrow metal-line systems do arise in quasar outflows. However, to identify individual NAL outflow systems we need more information. The most commonly used indicators of an outflow origin are line variability, resolved absorption profiles that are significantly broad and smooth compared to thermal linewidths or line strength ratios in multiplets that reveal partial line-of-sight covering of the background light source (Barlow & Sargent 1997; Hamann et al. 1997b; Misawa et al. 2007b; Hamann & Simon 2010; Simon & Hamann 2010).

Here we discuss a complex of five outflow NAL systems at velocities from -9710 to $-14\,050$ km s^{-1} in the redshift ~ 2.3 quasar J212329.46 $-$ 005052.9 (hereafter J2123 $-$ 0050). To our knowledge, these are the highest-velocity NALs whose outflow nature is confirmed by all three indicators of variability, partial covering and smooth superthermal line profiles. We selected this quasar from the Sloan Digital Sky Survey (SDSS) as part of a larger study of intervening, metal-strong damped Lyα (DLA) and sub-DLA absorption line systems (Herbert-Fort et al. 2006). Follow-up observations (Kaplan et al. 2010; Malec et al. 2010; Milutinovic, Prochaska & Tumlinson, in preparation) revealed the variability and outflow origin of the NAL systems discussed here. In the sections below we

Table 1. Observation Summary.

Year	Date (yyyy/mm/dd)	Telesc.	Resol. (km s^{-1})	$\Delta\lambda$ (Å)
2002.68	2002/09/06	SDSS	150	3805–9205
2006.64	2006/08/20	Keck	2.7	3057–5896
2006.71	2006/09/16	MMT	220	3050–4988
2008.61	2008/08/10	VLT	5.5	3047–3870
,,	,,	,,	4.5	4622–9466
2008.65	2008/08/27	VLT	,,	,,
2008.66	2008/08/30-31	VLT	,,	,,
2008.73	2008/09/22	VLT	,,	,,
2008.73	2008/09/25	VLT	,,	,,
2009.40	2009/05/25	MMT	220	3329–5968

describe the observations (Section 2), present measurements and analysis of the outflow lines (Section 3) and discuss the interpretation and broader implications of our results (Section 4). We provide a detailed general summary in Section 5. Throughout this paper, we adopt a cosmology with $H_o = 70$ km s^{-1} Mpc, $\Omega_M = 0.3$ and $\Omega_\Lambda = 0.7$.

2 OBSERVATIONS AND OTHER DATA

Table 1 summarizes the observations used in this study. Columns 1 and 2 give the fractional years and calendar dates of the observations. Columns 3–5 list the telescope, spectral resolution and wavelength coverage, $\Delta\lambda$, respectively. We obtained the 2002.68 spectrum from the SDSS archives fully reduced and calibrated. The fluxes provided by the SDSS are expected to be accurate to within a few per cent (Adelman-McCarthy et al. 2008). Unfortunately, these are the only reliable absolute fluxes available for our spectra.

We observed J2123−0050 at the MMT observatory using the MMT Spectrograph in 2006.71 and 2009.40. The resolutions and wavelength coverages listed in Table 1 were obtained using a 1.5-arcsec wide entrance slit together with the 800 groove mm^{-1} grating in the blue channel. We extracted and calibrated these spectra with standard techniques using the Low Redux Pipeline[1] software package. We performed relative flux calibrations using spectrophotometric standards observed on the same night.

The emission-line redshift of J2123−0050 reported by the SDSS, $z_e = 2.2614$, was modified recently to 2.2686 ± 0.0003 by Hewett & Wild (2010). These redshifts match the peak position of the broad C IV $\lambda\lambda$1548, 1551 emission line quite well. However, the lower ionization lines O I λ1303 and C II λ1336 appear at a slightly higher redshift that is probably closer to the true quasar systemic (within $\sim$100 km s^{-1}; Tytler & Fan 1992; Shen et al. 2007). We therefore estimate the redshift from the O I and C II lines as follows. First we average together the SDSS and MMT 2006.71 spectra to maximize the signal-to-noise ratio. Then we manually interpolate across the tops of any narrow absorption lines to eliminate these features (e.g. in the O I emission line profile), and calculate the O I and C II emission line centroids. This yields an average redshift for the two lines of $z_e = 2.278 \pm 0.002$ (using laboratory wavelengths from Verner, Verner & Ferland 1996). Measurements based on the line peaks or the centroids of only the upper halves of the profiles yield essentially the same result. Also, redshifts determined separately for the two lines agree within the measurement uncertainty quoted

above. We will adopt the redshift $z_e = 2.278 \pm 0.002$ for the quasar systemic throughout the remainder of this paper.

We observed J2123−0050 at high spectral resolutions at the W. M. Keck observatory using the High Resolution Echelle Spectrograph (HIRES) and at the Very Large Telescope (VLT) using the Ultraviolet and Visual Echelle Spectrograph (UVES). We extracted and calibrated the Keck spectra using the HIRES reduction package HIRedux.[2] More information about the Keck/HIRES observations and data reductions can be found in Milutinovic et al. (in preparation). We obtained the VLT/UVES spectra in separate blue and red channels covering the wavelengths indicated in Table 1. These data were reduced by the UVES data reduction pipeline. The final wavelength scales in both the Keck and VLT spectra are in the vacuum heliocentric frame. We combined the UVES spectra obtained in different Echelle orders and in different exposures using the customized code UVES_POPLER.[3] The VLT/UVES spectra were obtained on several dates during a $\sim$6-week period in 2008 (Table 1). A careful examination of these spectra shows that there are no significant differences in any of the absorption lines within this data set. Hereafter, we discuss only the average VLT spectrum referred to by the average date, 2008.67. This spectrum represents a total of 11.3 h of total exposure time on the quasar.

To measure the absorption lines, we define pseudo-continua in all of the spectra by manually drawing a smooth curve that matches the data in every important detail while extrapolating over the tops of the absorption lines. We then divide the original data by these pseudo-continua to obtain normalized spectra for our analysis below. This procedure works well redward of the Lyα emission line ($\lambda > 3985$ Å observed) in all of our data. However, in the lower resolution SDSS and MMT data, the blending of lines in the Lyα forest is too severe to yield useful results. We therefore exclude the SDSS and MMT data at these short wavelengths from our analysis.

2.1 Quasar properties

The photometric magnitudes reported by the SDSS (e.g. $r = 16.4$ and $i = 16.3$) indicate that J2123 − 0050 is one of the most luminous quasars known. (Inspection of the SDSS images reveals no evidence for gravitational lensing that might artificially boost the observed fluxes; Just et al. 2007, .) We estimate the bolometric luminosity of J2123 − 0050 to be $L = 8.4 \times 10^{47}$ erg s^{-1} based on the specific luminosity at 1450 Å in the rest frame of $\lambda L_\lambda(1450\,\text{Å};) \approx 1.9 \times 10^{47}$ erg s^{-1} (see Fig. 2 below) and a bolometric correction factor of $L = 4.4\,\lambda L_\lambda(1450\,\text{Å})$ (see the Appendix; also Warner, Hamann & Dietrich 2004). Combining this luminosity with our own measurement of the C IV emission linewidth, FWHM ≈ 8750 km s^{-1} from the SDSS spectrum, yields an estimate of the black hole mass, $M_{BH} \approx 2 \times 10^{10}$ M$_\odot$ (Vestergaard & Peterson 2006), and the Eddington ratio, $L/L_E \approx 0.4$, where L_E is the Eddington luminosity. These values of M_{BH} and L/L_E are within the nominal range of other high-luminosity quasars (Shemmer et al. 2004; Netzer et al. 2007).

Some of our analysis in Sections 3 and 4 below relies on size estimates for the quasar emission sources. If the UV continuum source is a geometrically thin accretion disc that emits like a blackbody at every radius, then the size of the continuum emitter at different wavelengths depends only on the bolometric luminosity and the radial run of temperature, $T(r)$, in the disc (Peterson 1997). The luminosity of J2123 − 0050 combined with $T(r) \propto r^{-0.57}$ (Gaskell

---

[1] http://www.ucolick.org/~xavier/LowRedux/index.html

[2] http://www.ucolick.org/~xavier/HIRedux/index.html
[3] http://astronomy.swin.edu.au/~mmurphy/UVES_popler.html

2008) indicates continuum source diameters of ~0.026 pc at 1550 Å and ~0.013 pc at 1034 Å (Hamann & Simon 2010). The radius of the C IV broad emission line region (BELR) should be roughly $R_{BELR} \sim 0.65$ pc based on the empirical scaling relation with luminosity (Bentz et al. 2007) as formulated by Hamann & Simon (2010).

2.2 Other data

Just et al. (2007) note that J2123 − 0050 is radio quiet based on a non-detection in the FIRST radio survey (Becker, White & Helfand 1995). They also report that J2123 − 0050 has a relatively 'soft' X-ray spectrum, with a power-law slope of $\alpha < -1.1$ ($f_\nu \propto \nu^\alpha$) from roughly 0.5–8 keV (observed frame) and no evidence for continuous X-ray absorption in the quasar environment. The short exposure time of the X-ray observations does not provide a strong upper limit on the column density of X-ray absorption. However, the X-ray characteristics of J2123 − 0050 are like other luminous radio-quiet quasars, for which Just et al. (2007) derive an upper limit of $N_H \lesssim 2 \times 10^{21}$ cm^{-2} on the X-ray absorbing column using coadded spectra of quasars in their sample. Consistent with a lack of X-ray absorption, J2123 − 0050 has a two-point power-law index of $\alpha_{ox} = 1.91$ between 2500 Å and 2 keV in the quasar frame, which is in the nominal range for luminous radio-quiet quasars with no X-ray absorption (Steffen et al. 2006; Just et al. 2007).

3 ANALYSIS AND RESULTS
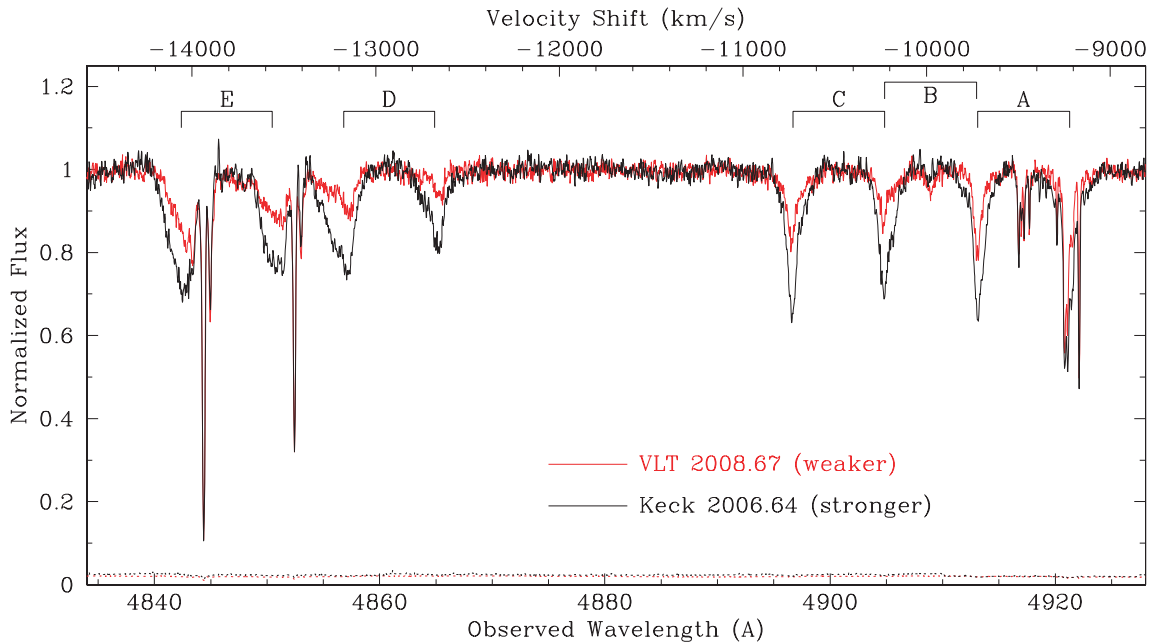
3.1 Defining the variable systems

Fig. 1 shows the five variable C IV $\lambda\lambda$1548, 1551 doublets (labelled A–E) in the normalized Keck 2006.64 and VLT 2008.67 spectra. Significant changes in the line strengths are clearly evident. It is

also evident that the changes were well coordinated between the five systems (see also Section 3.2 below).

Fig. 2 shows the variable C IV NALs in relation to other features in the J2123 − 0050 spectrum. The spectrum shown in this figure represents the product of the normalized Keck 2006.64 data times the pseudo-continuum drawn through the SDSS 2002.68 spectrum. A small featureless gap in the Keck wavelength coverage around 4970 Å (observed) is filled using the VLT spectrum. The result in Fig. 2 thus has the fluxes, broad emission lines and overall shape matching the SDSS data in 2002.68, but with the absorption lines measured at much higher resolution at Keck in 2006.64.

There are a number of other narrow C IV systems scattered across the J2123 − 0050 spectrum. They include one system at a smaller velocity shift than the variable lines (at ~4960 Å observed) and another that is blended with the variable system E (see also Fig. 1). Careful comparisons between the Keck and VLT spectra shows that none of these other narrow C IV systems varied significantly (e.g. by more than a few per cent in their rest equivalent widths) between the 2006.64 and 2008.67 observing epochs. Several C IV systems measured in the Keck spectrum appear at wavelengths not covered by the VLT data. For these systems, we searched for variability in all of the other data sets listed in Table 1. We again find no evidence for variability in the other lines, in this case above an estimated sensitivity threshold of ~20 per cent in the integrated line strengths. The only variable C IV lines detected in our data are the five systems labelled A–E in Figs 1 and 2.

One important property of the variable C IV lines is that they all reach significantly below the continuum shown by the dashed curve in Fig. 2. We estimate this continuum based on a single power-law fit constrained by the measured flux in narrow wavelength intervals (1437–1448, 1675–1700 and 1990–2030 Å rest) that avoid the broad emission lines. The power-law index of the fit is $\alpha = -0.67$ (for $f_\nu \propto \nu^\alpha$). The fact that the variable systems significantly absorb the quasar continuum is important because the partial line-of-sight

Figure 1. Normalized spectra of J2123 − 0050 showing the variable C IV systems A–E in the two high-resolution observations: 2006.64 (black curve) and 2008.67 (red). The velocity scale across the top applies to the short-wavelength lines in the doublet, C IV λ1548, relative to the emission redshift, $z_e = 2.278$. The 1σ variance spectra are plotted as dotted black and red curves across the bottom. Much narrower absorption lines not labelled are cosmologically intervening and unrelated to the variable outflow systems.
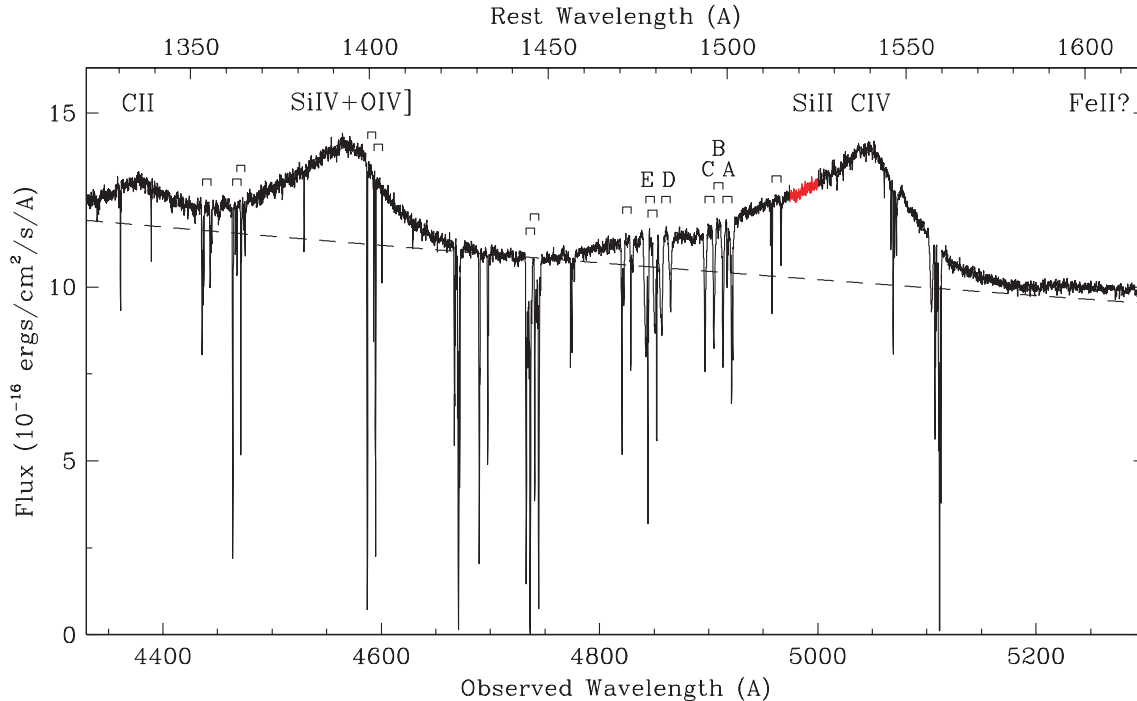
Figure 2. Synthesized spectrum of J2123 − 0050 showing the absorption lines in the Keck 2006.64 data relative to the broad emission lines and overall spectral shape defined by the SDSS measurement in 2002.68. All of the C IV λλ1548, 1551 absorption doublets detected in this wavelength range are marked by open brackets above the spectrum. The variable outflow systems are labelled A–E. Various broad emission lines are labelled across the top. A small featureless segment near 4970 Å observed (drawn in red) uses the average VLT 2008.67 spectrum to fill a small gap in the Keck wavelength coverage. The Keck and VLT spectra are shown after binomial smoothing to improve the presentation. The dashed curve is a power-law fit to the underlying quasar continuum.

covering deduced from the line ratios (Sections 3.3 and 3.4 below) applies to the continuum source and not (or not only) to the much larger BELR (Section 2.1).

Finally, we search for lines of other ions in the five variable systems using both the Keck 2006.64 and VLT 2008.67 data. This search is complicated for wavelengths below ∼1270 Å in the absorber frame because of contamination by the dense forest of unrelated (intervening) Lyα absorption lines. None the less, we find strong absorption in O VI λλ1032, 1038 in all five variable systems, probable absorption in N V λλ1239, 1242 in some of those systems and a secure detection of Lyα in system C. We note that the detection of O VI in system B confirms the reality of this system, which is not obvious from C IV alone because of the blending with systems A and C (see Figs 2 and 4 below). No other lines are detected in the variable systems, including specifically Lyβ and low-ionization metal lines such as C II λ1336, C III λ977, Si III λ1206 and Si IV λλ1394, 1403.

3.2 Line measurements and variability properties

Table 2 lists several parameters of the variable C IV lines A–E measured from the normalized Keck 2006.64 and VLT 2008.67 spectra. These results were obtained using cursor commands in the IRAF[4] software package. For comparison, Table 2 also lists measurements (from the Keck spectrum only) for the three non-variable C IV sys-

tems that are closest in velocity to systems A–E. Column 1 in the table gives the variable system name, where A+B and C+B refer to the blended C IV features. Column 2 identifies the line within the C IV doublet. For the blends A+B and C+B, the doublet line listed pertains to systems A and C, respectively, which appear to dominate the absorption based on our line fits in Section 3.3 below. Columns 3 and 4 give the observed wavelengths (λ_{obs}, vacuum heliocentric) and redshifts (z_a) of the line centroids. Column 5 lists the centroid velocities (v) relative to $z_e = 2.278$. Columns 6 and 7 give the rest equivalent widths (REW) and the full widths at half minimum (FWHM). The non-variable C IV systems at $z_a = 2.1291$ and $z_a = 2.1139$ each consists of two or more blended subcomponents. The table lists the total REWs for these blends while the FWHM pertains to the strongest single line in the blend.

For the variable systems A and E, we record the REWs and FWHMs in Table 2 after removing contributions from unrelated non-variable lines (see Figs 2, 4 and 5 below). This was achieved by extrapolating the A and E line profiles across the tops of the much narrower unrelated features. We are guided in this by the fact that the unrelated features did not vary between 2006.64 and 2008.67. Thus we can accurately decompose the blends into variable and non-variable components.

In the lower-resolution SDSS and MMT spectra, the C IV systems A+B+C and D+E are severely blended together. We therefore measure only the total REWs in these blends for comparison to the Keck and VLT measurements. We also correct the total SDSS and MMT REWs for small contributions from the non-variable lines that are blended with systems A and E (as measured from the Keck and VLT spectra). Fig. 3 plots the total C IV REWs in systems A+B+C and D+E at each observed epoch. The vertical bars in the figure are estimates of the 1σ uncertainties associated with each REW

---

[4] IRAF is distributed by the National Optical Astronomy Observatory, which is operated by the Association of Universities for Research in Astronomy (AURA) under cooperative agreement with the National Science Foundation.

Table 2. C IV line measurements.

System	Line	2006.64 Keck λ_{obs} (Å)	z_a	v (km s^{-1})	REW (Å)	FWHM (km s^{-1})	2008.67 VLT λ_{obs} (Å)	z_a	v (km s^{-1})	REW (Å)	FWHM (km s^{-1})
A	1551	4921.3	2.17343	−9716	0.150	62	4921.3	2.17342	−9717	0.063	55
A+B	1548	4913.2	2.17349	−9710	0.156	66	4913.2	2.17348	−9711	0.061	50
C+B	1551	4905.0	2.16291	−10710	0.144	85	4905.0	2.16295	−10707	0.055	36
C	1548	4896.7	2.16284	−10717	0.162	62	4896.7	2.16285	−10716	0.082	53
D	1551	4865.0	2.13712	−13162	0.115	100	4865.3	2.13731	−13144	0.024	62
D	1548	4856.5	2.13689	−13184	0.209	164	4856.6	2.13694	−13179	0.075	111
E	1551	4850.6	2.12788	−14045	0.180	147	4850.4	2.12775	−14056	0.114	142
E	1548	4842.4	2.12776	−14056	0.245	154	4842.8	2.12799	−14034	0.133	121
	1551	4966.3	2.20246	−6987	0.024	27.1	—	—	—	—	—
	1548	4958.1	2.20247	−6986	0.042	27.2	—	—	—	—	—
	1551	4852.5	2.12909	−13930	0.077	14.2	—	—	—	—	—
	1548	4844.5	2.12910	−13928	0.123	17.3	—	—	—	—	—
	1551	4829.0	2.11395	−15380	0.090	23.6	—	—	—	—	—
	1548	4821.0	2.11394	−15382	0.163	26.1	—	—	—	—	—
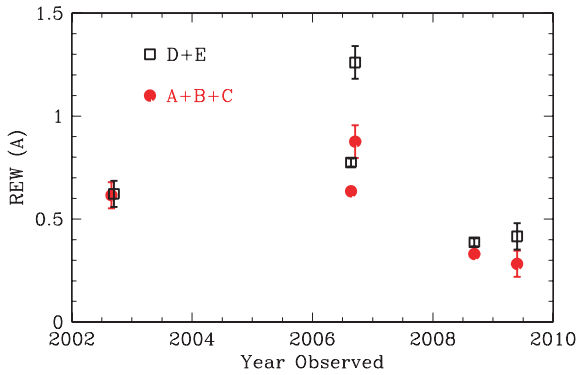
Figure 3. The total rest equivalent widths (REW) of the variable C IV systems A+B+C (filled red circles) and D+E (open black squares) are shown for each year observed. The vertical bars indicate approximate 1σ uncertainties in the REW measurements.

measurement. These errors are dominated by the pseudo-continuum placement. We estimate the uncertainties by making repeated measurements of the REWs using different plausible continuum heights.

One surprising result in Fig. 3 is that the REWs differ dramatically between the Keck 2006.62 and MMT 2006.71 spectra obtained only ∼1 month apart in the observed frame. These REW differences are also evident from direct comparisons of the normalized spectra (not shown). They have a formal significance of 3σ for systems A+B+C and 6σ for D+E (based on the uncertainties shown in Fig. 3). We carefully reviewed our pseudo-continuum placements across these lines and found no evidence for uncertainties larger than those depicted in Fig. 3. None the less, we consider this evidence for dramatic short-term REW changes to be tentative because of the inherent difficulties in comparing the strengths of weak absorption lines in spectra with vastly different resolutions. In this case, the much shallower appearance of the blended lines in the lower-resolution data makes them more susceptible to uncertainties in the pseudo-continuum placement that might be caused, for example, by small changes in the underlying emission line spectrum. We also note that significant line variations did not occur between our much more precise VLT measurements obtained over a similar period of ∼1.5 months in 2008 (Table 1).

Figs 4 and 5 compare the normalized high-resolution Keck and VLT spectra across the variable C IV and O VI systems. The O VI lines are severely blended with unrelated features in the Lyα forest. None the less, the O VI outflow lines are clearly identified by their variability and their distinctive profiles and redshift agreement with C IV. Notice that the O VI lines are both stronger and broader than the C IV features, with variable absorption that appears to extend across a wider range of velocities compared to C IV.

Fig. 6 shows the Keck and VLT spectra across Lyα in the variable systems A, B and C. Lyα is clearly detected only in system C, based on its good match to the redshift, absorption profile and variability characteristics of C IV. Lyα is significantly not present in system B, while its strength in the other systems (including D and E, not shown) is poorly constrained because of line blending problems.

3.3 Covering factors and column densities

The smooth green and blue curves in Figs 4–6 are fits to the variable line profiles. These fits assume that at each velocity, v, a spatially homogeneous absorbing medium covers a fraction, $0 < C_v \leq 1$, of a spatially uniform emission source. In this situation, the line intensities seen by a distant observer are given by

$$\frac{I_v}{I_c} = (1 - C_v) + C_v e^{-\tau_v}, \tag{1}$$

where I_c is the unabsorbed source intensity and τ_v and C_v are the line optical depth and covering fraction, respectively (see Ganguly et al. 1999; Hamann & Ferland 1999; Hamann & Sabra 2004, for more general formulations). We can solve equation (1) for τ_v and C_v at each v using the intensity ratios of lines within multiplets, such as C IV $\lambda\lambda$1548, 1551, where the optical depth ratio is known from the atomic physics, in this case $\tau_{1548}/\tau_{1551} \approx 2.0$ (see also Barlow & Sargent 1997; Hamann et al. 1997b). For the resonance transitions discussed here, and assuming the ions that are entirely in their ground states, the ionic column densities are given by

$$N_{ion} = \frac{m_e c}{\pi e^2 f \lambda_o} \int \tau_v \, dv, \tag{2}$$

where f and λ_o are the line oscillator strength and laboratory wavelength, respectively (Savage & Sembach 1991).

Previous studies have shown that τ_v and C_v can both have complex velocity-dependent behaviours that differ significantly between
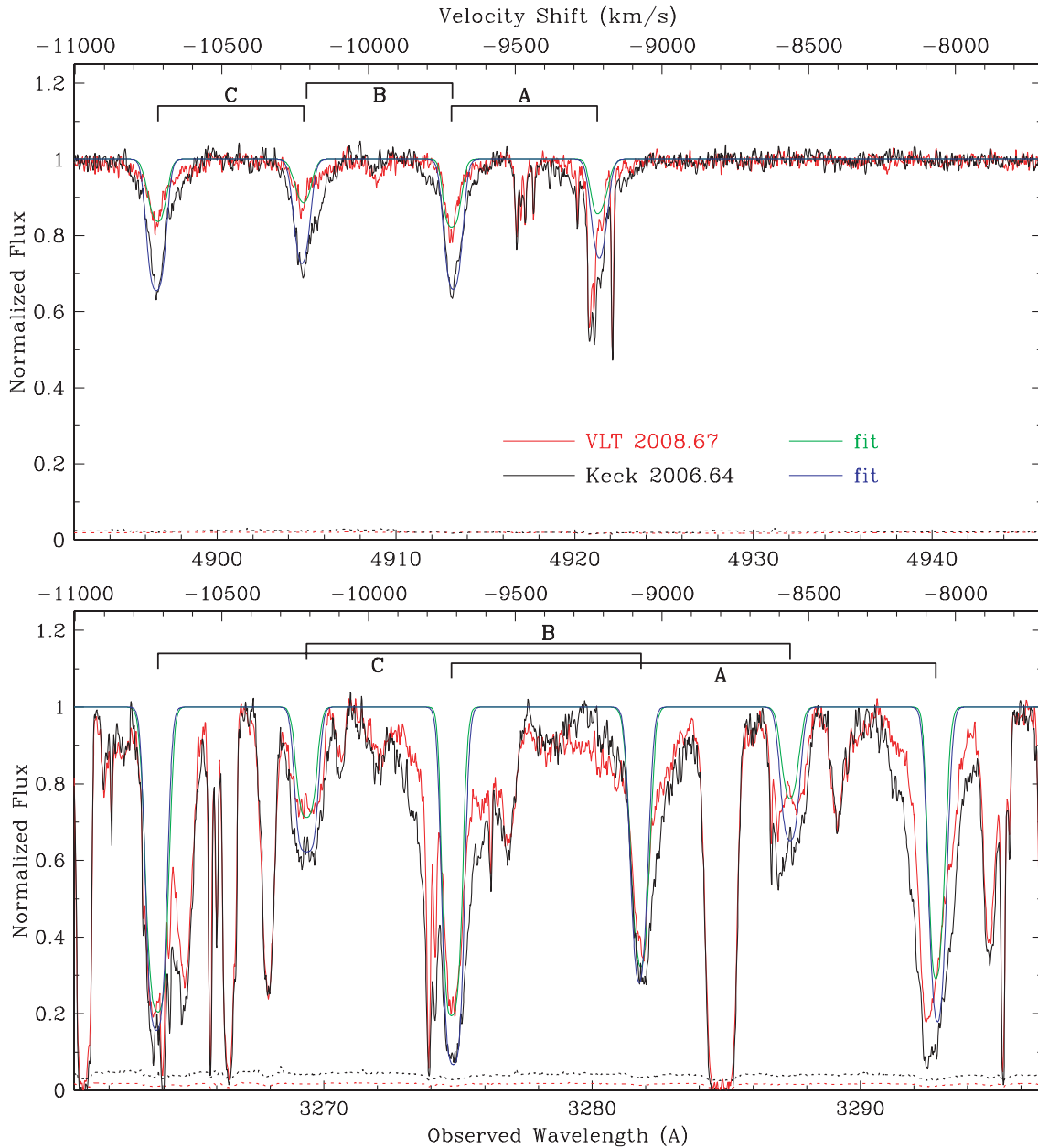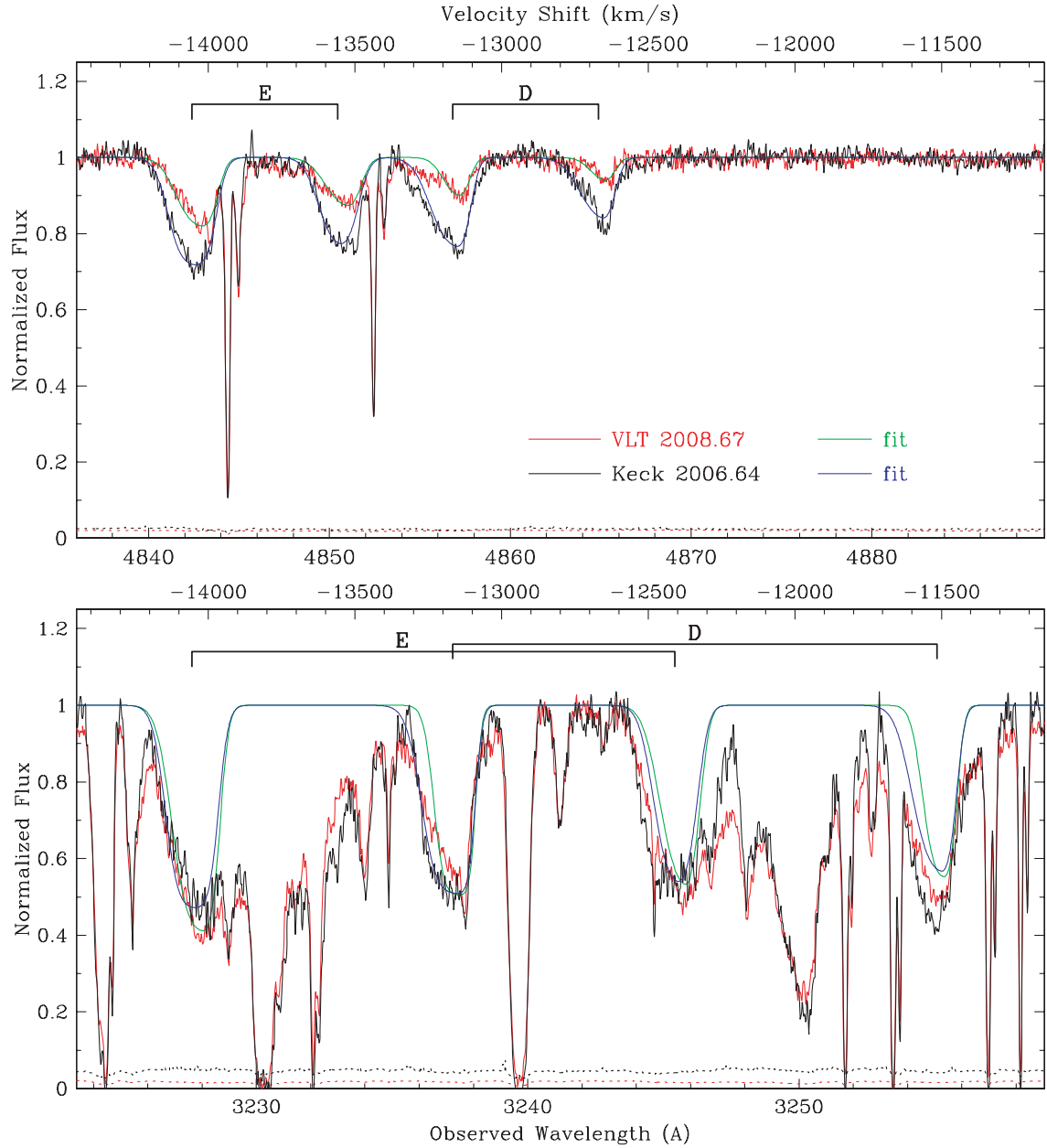
Figure 4. Normalized spectra showing the C IV (top panel) and O VI (bottom) doublets in the variable systems A, B and C as observed in the Keck 2006.64 (black curve) and VLT 2008.67 (red) data. The doublet positions are shown by the brackets above the spectra. Many unrelated absorption lines are present in the O VI plot caused by the Lyα forest and by a system of extremely narrow H_2 features in an intervening galaxy at $z = 2.059$ (Malec et al. 2010). The velocity scale across the top of each panel applies to the short-wavelength lines in the doublets, C IV 1548 and O VI 1032, relative to the emission redshift, $z_e = 2.278$. The smooth blue and green curves are fits to the variable lines in the Keck and VLT data, respectively, as described in Section 3.3. The dotted curves across the bottom are the 1σ uncertainties.

lines and between ions (Barlow & Sargent 1997; Hamann et al. 1997b, 2001; Ganguly et al. 1999; Hamann & Sabra 2004; Arav et al. 2005; Arav et al. 2008; Gabel et al. 2005; Gabel, Arav & Kim 2006). Unfortunately, blending problems prevent us from obtaining v-dependent solutions to equations (1) and (2) for most lines in the variable systems A–E. We therefore adopt a parametrized approach that involves (i) fitting the C IV profiles with constant values of the covering fractions, $C_v = C_o$, across the line profiles, and then (ii) shifting and scaling the C IV fits to place constraints on other lines. This procedure also has the advantage of avoiding potentially large uncertainties in C_v, τ_v and therefore N_{ion} that can be introduced by

noise, e.g. in the line wings, when solving equation (1) point by point at each v across the line profiles. The reliability of our fitting procedure is discussed further at the end of this section (see also Simon & Hamann 2010).

Our fits assume Gaussian τ_v profiles with potentially different values of the doppler width parameter on either side of line centre. This functional form provides flexibility to account for some of the asymmetry in the measured lines, while still preserving a simple relationship between N_{ion} and the line centre optical depth, τ_o, namely,

$$N_{ion} = 3.34 \times 10^{14} \left(\frac{b_b + b_r}{f\lambda_o} \right) \tau_o \quad cm^{-2}, \tag{3}$$

Figure 5. Normalized spectra showing the C IV (top panel) and O VI (bottom) doublets in the variable systems D and E. See Fig. 4 caption.

where λ_o is the lab wavelength in Å, and b_b and b_r are the blue and red side doppler parameters, respectively, in km s^{-1}. Each doublet pair is forced to have the same doppler parameters, velocity shift and a 2:1 ratio in the line optical depths.

Our initial attempts to fit the C IV profiles using a χ^2 minimization technique led to spurious results. We found that manual adjustments and iteration by trial and error provide more flexibility and a much better understanding of the uncertainties in situations like this where the line profiles are irregular and the blending is potentially severe (e.g. in the C IV systems A+B+C).

The fit results in Figs 4 and 5 show that the asymmetric Gaussians provide a good match to the C IV profiles in systems D and E, but they are not able to produce simultaneously the narrow cores and extended wings in systems A, B and C. We choose the 'best' fits by giving highest priority to matching the line cores because they are most important for the accuracy of key parameters, τ_o, C_o and

N_{ion}. Note that the amount of C IV absorption contributed by the fully blended system B is highly uncertain. The line ratios across the blend A+B+C indicate that the amount of C IV absorption in system B is less than A and C. Repeated attempts to fit C IV in the three systems A, B and C simultaneously[5] indicate that system B

---

[5] There is no straightforward way to combine the intensities of blended lines with partial covering because the absorbing regions can have different values of C_v across different spatial locations in front of the emission source. Our treatment assumes the maximum amount of spatial overlap between absorbing regions. For example, if absorbing regions 1 and 2 have covering fractions $C_1 > C_2$ and line optical depths τ_1 and τ_2, respectively, then the total covering fraction is C_1. The total line optical depth is $\tau_1 + \tau_2$ in the spatial overlap region with covering fraction C_2, and τ_1 in the non-overlap region with covering fraction $C_1 - C_2$. See Hall et al. (2003, 2007) for more examples and illustrations.
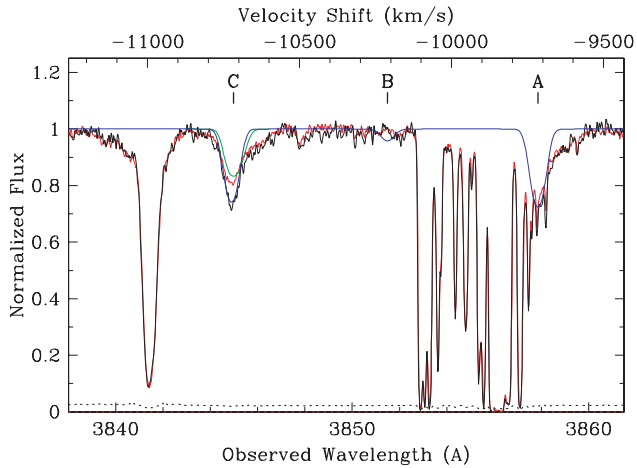
Figure 6. Normalized spectra obtained at Keck (2006.64, black curve) and the VLT (2008.67, red) showing the Lyα line in the variable systems A, B and C. Other absorption lines, not labelled, are unrelated features formed in the intervening clouds or galaxies. See Fig. 4 caption.

might contribute up to ~30 per cent of the total REW in the lines at this location. However, the data are also consistent with no C IV contribution from system B at all. Therefore, none is included in the final fits shown in Fig. 4 (also Table 3 below).

Table 3 lists the C IV fit parameters derived from the Keck (2006.64) and VLT (2008.67) spectra. Columns 1 and 2 indicate the system names and the observation years. Columns 3 and 4 give the redshifts, z_o, and velocity shifts, v_o, of the Gaussian centres. (Note that these are not centroid positions unless the profile is symmetric.) Columns 5 and 6 list the blue and red side doppler parameters. Column 7 gives the line-centre optical depths for the stronger λ1548 transition. Column 8 lists the covering fractions, and column 9 provides the ionic column densities from equation (3). We estimate 1σ uncertainties in these quantities by trial-and-error experiments with different fit parameters and different pseudo-continuum levels. The uncertainties in v_o, b_r and b_b should be ~3 km s^{-1} in systems A and C and roughly double that in the broader systems D and E. The covering fractions are in all cases well constrained, with errors of <10 per cent. The optical depths and column densities have nominal 1σ uncertainties around 25 per cent. Including a maximum possible contribution from system B would lead to lower values of τ_o and N_{ion} in systems A and C by about 30 per cent.

Next we transfer the C IV fits to other lines in the variable systems by keeping the kinematic parameters v_o, b_b and b_r fixed while scaling only τ_o and C_o, as needed. For system B, we adopt $v_o = -10210$ km s^{-1} and $b_r = b_b = 30$ km s^{-1} based on our efforts to add a system B contribution to the C IV blend. This simple

Table 4. Additional fit results.

Line	System	Year	C_o	N_{ion} (10^{13} cm^{-2})
O VI	A	2006.64	0.95	>58.4
O VI	A	2008.67	0.82	>53.5
O VI	B	2006.64	0.38	>58.4
O VI	B	2008.67	0.30	>58.4
O VI	C	2006.64	0.87	51.1
O VI	C	2008.67	0.82	55.4
O VI	D	2006.64	0.50	>136
O VI	D	2008.67	0.50	>102
O VI	E	2006.64	0.54	>136
O VI	E	2008.67	0.63	92.0
Si IV	A	2006.64	—	<0.30
Si IV	B	2006.64	—	<0.30
Si IV	C	2006.64	—	<0.30
Si IV	D	2006.64	—	<0.60
Si IV	E	2006.64	—	<0.60
N V	A	2006.64	—	—
N V	B	2006.64	—	<8.5
N V	C	2006.64	—	<18
N V	D	2006.64	—	—
N V	E	2006.64	—	<72
H I	A	2006.64	—	<5.2
H I	B	2006.64	—	<0.6
H I	C	2006.64	—	4.8
H I	C	2008.67	—	7.7
H I	D	2006.64	—	<6.4
H I	E	2006.64	—	<23
C III	A	2006.64	—	<5.0
C III	B	2006.64	—	<3.0
C III	C	2006.64	—	<3.0
C III	D	2006.64	—	<15
C III	E	2006.64	—	<15

shift-and-scale approach is essential for dealing with non-detections and blends in the Lyα forest. It is also justified by the good results shown for O VI and Lyα in Figs 4–6. However, as noted in Section 3.2 above, the O VI absorption appears to span a wider range of velocities than C IV. Our fits ignore this additional O VI absorption because (i) it is poorly measured due to blending problems, and (ii) we want to limit our comparisons between C IV and O VI to the same kinematic gas components anyway, for the ionization and abundances analysis in Sections 3.6 and 3.7 below.

Table 4 lists the fit parameters derived for the other lines. The O VI doublets measured in 2006.64 and 2008.67 provide useful constraints on both C_o and N_o. Notice that the O VI covering fractions are larger than C IV (cf. Table 3). Also note that several of the O VI

Table 3. C IV fit results.

System	Year	z_o	v_o (km s^{-1})	b_b (km s^{-1})	b_r (km s^{-1})	τ_o	C_o	N_{ion} (10^{13} cm^{-2})
A	2006.64	2.17350	−9709	30	30	2.3	0.38	15.7
A	2008.67	2.17344	−9715	30	25	2.8	0.19	17.5
C	2006.64	2.16278	−10723	30	30	2.7	0.37	18.4
C	2008.67	2.16284	−10717	30	35	1.0	0.20	12.5
D	2006.64	2.13727	−13148	95	45	1.5	0.30	23.8
D	2008.67	2.13733	−13142	65	40	0.8	0.18	9.54
E	2006.64	2.12790	−14043	80	60	2.8	0.30	44.5
E	2008.67	2.12816	−14018	90	50	1.7	0.22	27.0

doublets are saturated, with intensity ratios close to unity (see Figs 4 and 5). For these systems, Table 4 lists lower limits on the column densities that correspond to $\tau_o = 4$ in the stronger O VI $\lambda 1032$ line. The values of N_{ion} listed for O VI system C and system E in 2008.67 (only) come from fits indicating $\tau_a o < 4$. However, we could conservatively consider all of the O VI column densities to be lower limits because of the blending problems in the Lyα forest. We estimate 1σ uncertainties in the O VI results by repeating the fits with different continuum placements while keeping z_o and the doppler parameters fixed, as described above. We find that the errors in C_o are <15 per cent while the errors in N_{ion} are roughly 30 per cent. We conclude that the differences in the derived covering fractions between O VI and C IV, and the smaller changes in the O VI covering fractions compared to the changes in C IV (cf. Tables 3 and 4), both have a large significance.

The remaining lines listed in Table 4 are either non-detections (Si IV and C III) or severe blends (N V and H I) where we cannot use line intensity ratios to determine both τ_o and C_o. We therefore fix C_o along with the kinematic parameters and scale only τ_o to derive constraints on N_{ion}. Fig. 6 shows examples of these fits applied to Lyα in systems A, B and C. We adopt values of C_o from C IV (Table 3) in all cases except for Lyα in system B, which has no C IV fit result, and N V, which has measured lines/blends too deep to be consistent with C_o in C IV. For these latter cases we adopt the covering fractions from O VI. Two of the entries for N V in Table 4 are blank because the blending is too severe to yield meaningful results. The remaining three N V systems (B, C and E) are listed as upper limits in Table 4 because of blending uncertainties. We note, however, that there do appear to be real N V lines present with redshifts and profiles similar to C IV. The upper limits on N_{ion} listed for H I in Table 4 use the best available constraints from either Lyα or Lyβ. The specific values of the H I column density given for system C come from the Lyα fits shown in Fig. 6 without additional constraints from Lyβ. The errors in these H I results might be as large as a factor of ~ 2 due mainly to the uncertainties in C_o.

As a further check of our fitting analysis, we derive velocity-dependent values of τ_v and C_v for the two best-measured cases: the C IV lines in systems D and E observed in 2006.64. Specifically, we calculate the average line intensities in velocity bins 25 km s^{-1} wide and then solve equation (1) for τ_v and C_v in each bin. Fig. 7 compares the derived values of $1 - C_v$ to the observed line profiles. The vertical bars running through the filled circles in Fig. 7 represent 1σ uncertainties in C_v caused by photon statistics (Hall et al. 2003). However, in the blue wings of both systems D and E there are several velocity bins where the doublet ratios indicate $\tau_v \ll 1$ and the standard analysis yields $C_v = 1$. The actual values of τ_v and C_v are poorly constrained in these cases because the right-hand side of equation (1) reduces to $1 - C_v \tau_v$ in the $\tau_v \ll 1$ limit and, therefore, the line intensities constrain only the product $C_v \tau_v$ instead of C_v and τ_v separately. For example, in the velocity bin centred at $v = -13250$ km s^{-1} in C IV system D, the data are consistent with solutions ranging from $1 - C_v = 0$ and $\tau_v(1548) = 0.14$ to $1 - C_v \approx 0.5$ and $\tau_v(1548) = 0.28$. Fig. 7 shows both the maximum and minimum ($1 - C_v = 0$) results, connected by a vertical bar, for each of the optically thin data points. The data at these velocities are compatible with any value of $1 - C_v$ within the ranges shown.

The values of C_v and τ_v derived from the point-by-point analysis near line centre agree well with the C_o and τ_o obtained above from the Gaussian fits (Table 3). The point-by-point results in Fig. 7 show further that C_v changes significantly across the line profiles. In particular, the shape of the intensity profile across the core of system E appears to be governed largely by the behaviour of C_v
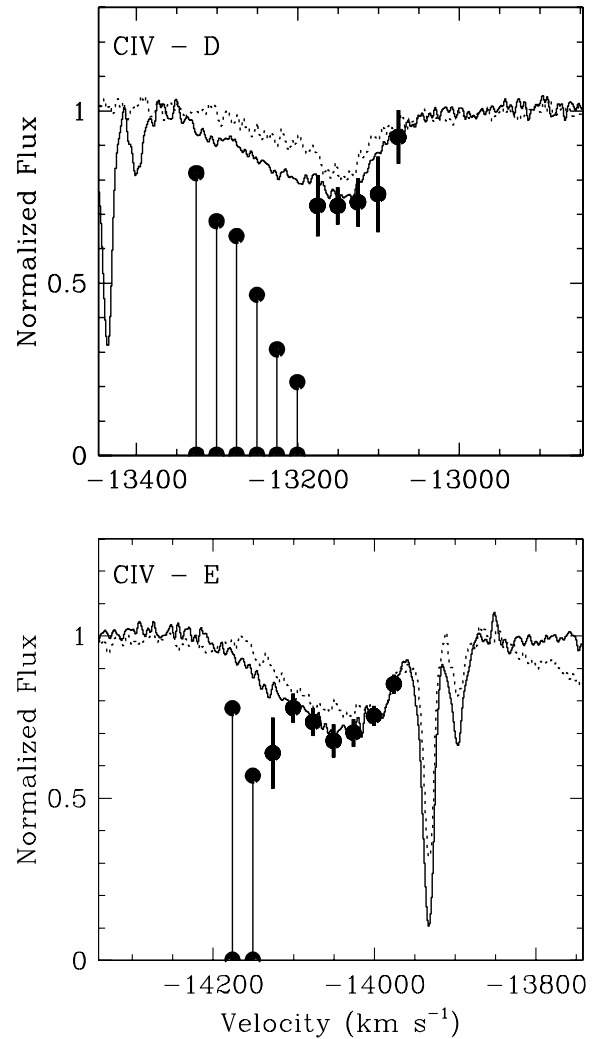
Figure 7. C IV line profiles measured in 2006.64 in systems D (top panel) and E (bottom), compared to the derived values of $1 - C_v$ (filled circles), on a velocity scale relative to $z_e = 2.278$. The solid and dashed curves show the stronger ($\lambda 1548$) and weaker ($\lambda 1551$) doublet members, respectively, after smoothing the spectra three times with a binomial function. The vertical bars on the filled circles are 1σ uncertainties. For the velocity bins with $\tau_v \ll 1$ (in the blue line wings), two filled circles at each velocity represent the full range of $1 - C_v$ values consistent with the data.

with $\tau_v > 2$. In system D, there appears to be an abrupt change in C_v around -13200 km s^{-1}, between a line core that has $\tau_v > 1$ and $C_v \approx 0.28$ and a blue wing with $\tau_v \ll 1$ and $C_v \approx 1$. Integrating τ_v over all of the velocity bins shown in Fig. 7 (as per equation 2 but excluding the lowest v point in the red wing of both systems because they formally yield $\tau_v \gg 1$ due to noise) indicates $N_{ion} = 2.3 \pm 0.3 \times 10^{14}$ cm^{-2} for system D and $3.8 \pm 0.3 \times 10^{14}$ cm^{-2} for system E. These column densities are in excellent agreement with the Gaussian fit results in Table 3.

We conclude with a comment about the assumption of spatial uniformity in the absorbing regions. Some studies of partial covering in quasar absorption lines indicate that the actual absorbing structures are inhomogeneous, with a range of τ_v values at each v across the projected area of the emission source (Hamann et al. 2001; de Kool, Korista & Arav 2002; Hamann & Sabra 2004; Arav et al. 2008, and references therein). The evidence for this is significantly different covering fractions in different lines/ions. While these data can

provide important constraints on the nature of the absorber inhomogeneities, there is not enough information to determine uniquely the two-dimensional spatial distributions of τ_v in each line. The situation is further complicated by the fact that the background light sources, e.g. the accretion disc and/or the BELR, have their own spatial non-uniformities that can include a wavelength-dependent size. A good strategy, therefore, is to consider the observational consequences of different plausible τ_v spatial distributions (de Kool et al. 2002; Hamann & Sabra 2004; Arav et al. 2005; Arav et al. 2008). In one study, extensive simulations using different functional forms for the τ_v spatial distribution show that equation (1) (which assumes a top hat τ_v distribution) yields good approximations to the spatially averaged values of τ_v and N_{ion} in more general inhomogeneous absorbing media (Hamann & Sabra 2004). Therefore, the results derived from equation (1) are appropriate for making spatially averaged estimates of the ionization and metal abundances (Section 3.6 below). They are also useful for characterizing the covering fractions even for complex absorbers. In particular, the values of C_v derived from equation (1) correspond roughly to the amount of coverage by absorbing material with $\tau_v \gtrsim 1$ in an inhomogeneous medium (Hamann & Sabra 2004).

3.4 Absorbing region sizes

The partial covering discussed in Section 3.3 implies that the absorbing structures are not much larger than the background light source. (The absorbers could be smaller than the emission source, but partial covering by much larger clouds would require unphysically sharp edges and extremely unlikely spatial alignments.) Fig. 2 shows that the variable C IV systems lie in the far blue wing of the C IV BEL, where the flux is dominated by continuum emission. In principle, the line absorption could occur in front of both the UV continuum source and the BELR, with potentially different covering fractions for each region (Ganguly et al. 1999). However, the depths of the lines below the quasar continuum (Fig. 2) imply that the C IV partial covering results pertain mostly or exclusively to the continuum source. This conclusion is confirmed by the O VI lines, which have even deeper absorption troughs and no significant underlying BELR flux.

The extent to which the absorbers cover the BELR are thus undetermined by our data. This ambiguity introduces a small additional uncertainty in C_v derived for the C IV lines because the BELR contributes roughly 10 per cent of the total flux at those wavelengths (Fig. 2). Our analysis in Section 3.3 assumed implicitly that C_v is the same for all emission sources beneath the absorption lines. However, if the BELR is not covered at all, the continuum covering fractions would be roughly 10 per cent larger than the values listed for C IV in Table 3. Conversely, if the C IV absorber completely covers the BELR, the continuum covering fractions would be ~20 per cent smaller than the results listed in Table 3 (see equations in Ganguly et al. 1999). This latter situation (complete coverage of the BELR with partial covering of the continuum source) seems highly unlikely given that the C IV BELR is of order 20 times larger than the continuum source at 1550 Å (Section 2.1). Hereafter, we will assume that all of the derived covering fractions apply only to the continuum source.

Comparing the covering fractions in C IV and O VI (Tables 3 and 4) to the theoretical diameters of the continuum source at 1550 and 1034 Å, respectively (Section 2.1), indicates that the C IV and O VI absorbing regions both have characteristic sizes of order ~0.01–0.02 pc (as measured in 2006.64). It is important to keep in mind, however, that this characteristic size is actually just an upper limit

on the true sizes of absorbing structures in the flow. In particular, partial covering might be caused by patchy distributions of many smaller substructures (see Section 4.4 below; see also Hamann & Sabra 2004).

3.5 Outflow dynamics

The five distinct outflow systems span a range of velocities from -9710 to $-14\,050$ km s^{-1} and C IV linewidths from FWHM ≈ 62–164 km s^{-1} (Table 2). The O VI lines, representing higher ionization material, appear somewhat broader than C IV in terms of both their FWHMs and broad weak wings (see Figs 4 and 5). The outflow systems have a natural division into two groups, A+B+C and D+E, based on similarities in the line strengths, profiles and velocity shifts (see also Fig. 1). One remarkable characteristic of these systems overall is their small velocity dispersions compared to the high flow speeds, e.g. FWHM/$v \sim 100$. This is in marked contrast to BAL outflows, which typically have FWHM/$v \sim 1$ (Weymann et al. 1991; Korista et al. 1993).

The kinematic stability of the narrowest systems A, B and C between 2006.64 and 2008.67 places an upper limit on the radial acceleration of $\lesssim 3$ km s^{-1} yr^{-1} in the quasar frame. We obtain this estimate from the measurements in Table 3 and by careful comparisons of simultaneous fits to all three narrow systems (in C IV and O VI) in both epochs. (The centroids of the broader systems D and E did change slightly between observations, but this appears to be the result of profile changes rather than a true velocity shift; Fig. 5.) For comparison, the gravitational acceleration due to M_{BH} at the radius of the C IV BELR (Section 2.1) is roughly 200 km s^{-1} yr^{-1}. Therefore, the outward driving force is either in a delicate balance with gravity or, more likely, the absorbing gas is located in a low-gravity environment farther from the black hole than the C IV BELR. A radial distance of $R \gtrsim 5$ pc is needed for the local gravity to be less than the observed acceleration limit. At this distance, the observed outflow speeds vastly exceed the local gravitational escape speed. Thus it appears that the absorbing gas is gravitationally unbound and coasting freely at speeds near the outflow terminal velocity.

There is an apparent occurrence of 'line-locking' between the narrow C IV systems A, B and C. In particular, the velocity differences between systems A–B and B–C are a close match to the C IV doublet separation of $\Delta v = 498$ km s^{-1}. (Although the system B lines are entirely blended in C IV, their velocity is confirmed by our fits to the O VI lines shown in Fig. 4.)

Line-locking is usually interpreted as evidence for radiative acceleration (Foltz et al. 1987; Braun & Milgrom 1989; Srianand & Petitjean 2000; Srianand et al. 2002; Ganguly et al. 2003). Cases of multiple line-locks between systems with narrow profiles, as in J2123 $-$ 0050, provide the best evidence for physically locked systems because they are difficult to explain by chance alignments of lines in the spectrum. However, it is not known if radiative forces can actually lock doublets like C IV together in real quasar outflows. The most plausible scenario was outlined by Braun & Milgrom (1989): Consider two blobs of gas moving along the same radial path in a radiatively accelerated outflow. The faster blob is farther from the emission source and experiencing a *greater* outward acceleration. When the velocity difference between the blobs matches the C IV doublet separation, $\Delta v \approx 498$ km s^{-1}, the $\lambda 1551$ line in the outer blob falls in the shadow cast by $\lambda 1548$ in the slower inner blob. This leads to diminished acceleration in the outer blob and a velocity lock between the two blobs at the doublet separation. Line-locking might even contribute to the formation of blobs because the localized dip in the radiative force downstream from the inner

blob creates a natural collecting area for outflow gas (Ganguly et al. 2003). This scenario does not require that the C IV lines dominate the overall acceleration, only that the acceleration transferred to the outer blob via the $\lambda 1551$ line is at least as large as the acceleration *difference* between the two blobs in the absence of shadowing (i.e. outside of the $\Delta v \approx 498$ km s^{-1} line overlap situation). The appearance of a double line-lock in C IV, as in J2123 $-$ 0050, might also be facilitated by the N V absorption doublet whose separation, $\Delta v = 964$ km s^{-1}, is close to the velocity difference between systems A and C. In any case, the feasibility of this line-lock interpretation has not been demonstrated in any quasar outflow.

Here we note simply that if radiative forces did indeed lock the C IV doublets in J2123 $-$ 0050, then the absorbing clouds must be moving almost directly towards us. This is because the velocity difference between line-locked blobs should match the C IV doublet separation along the flow direction. If the flow is not aimed directly at us, we should observe velocity differences between the systems that are smaller than the doublet separation. Our measurements of the line centroids (Table 2) and our fits to the profiles, including O VI in system B (Table 3 and Fig. 4), indicate that the velocity differences between systems A, B and C are within $\sim$20 km s^{-1} of $\Delta v = 498$ km s^{-1}. This implies that the absorber trajectories are within $\sim$16° of the purely radial (line-of-sight) direction.

3.6 Physical conditions

The strong detections of O VI compared to C IV absorption, and the non-detections of lower ionization lines like Si IV and C III (Tables 3 and 4), indicate that the degree of ionization is high and approximately the same in all of the variable systems. The Appendix below describes numerical simulations using the code CLOUDY (Ferland et al. 1998) of the ionization and physical conditions in clouds that are in photoionization equilibrium with a quasar continuum source. Comparing those results (Fig. A1) to the most stringent limit on the observed $N(\text{C III})/N(\text{C IV}) \lesssim 6$ column density ratio (system C in 2006.64) indicates that the dimensionless ionization parameter is at least $\log U \gtrsim -0.8$. The measured ratios of $N(\text{O VI})/N(\text{C IV}) \gtrsim 3$ provide a very similar constraint on $\log U$ if we make the additional assumption that the O/C abundance is approximately solar.

This lower limit on the ionization combined with the average measured H I column density in system C, $N(\text{H I}) \sim 6 \times 10^{13}$ cm^{-2} (Table 4), implies that the minimum total hydrogen column density in that system is $N_{\text{H}} \gtrsim 3 \times 10^{18}$ cm^{-2} (see Fig. A1). In Section 4.3 below, we argue that the line changes were caused by changes in the degree of ionization and the most likely value of the ionization parameter is $\log U \sim -0.4$, near the peak in the O VI ion fraction. Using that result, our best estimate of the actual total column density in system C is of order $N_{\text{H}} \sim 10^{19}$ cm^{-2}. Given the similarities between the systems A–E, we crudely estimate that the total column density in all five outflow absorbers is $N_{\text{H}} \sim 5 \times 10^{19}$ cm^{-2}.

The more conservative requirement for $\log U \gtrsim -0.8$ in a photoionized gas at $R \gtrsim 5$ pc (Section 3.5) from the quasar places an upper limit on the volume density of $n_{\text{H}} \lesssim 2 \times 10^{8}$ cm^{-3} (see equation A1). A lower limit on the density can be derived by noting that, in photoionization equilibrium, changes in the ionization state require at least a recombination time given by $t_{\text{r}} \approx (\alpha_{\text{r}} n_{\text{e}})^{-1}$, where n_{e} is the electron density and α_{r} is the recombination rate coefficient. Given $\alpha_{\text{r}} \approx 10^{-11}$ cm^3 s^{-1} for either O VII $\rightarrow$ O VI or O VI $\rightarrow$ O V at a nominal gas temperature of $T_{\text{e}} \approx 20\,000$ K (see Arnaud & Rothenflug 1985; Hamann et al. 1995), the observed O VI variability in $\leq$0.63 yr indicates a minimum density of $n_{\text{e}} \sim n_{\text{H}} \gtrsim 5000$ cm^{-3}.

This density combined with the ionization constraint $\log U \gtrsim -0.8$ yields a maximum distance of $R \lesssim 1.1$ kpc (equation A1).

The density and distance constraints based on the recombination time ($n_{\text{H}} \gtrsim 5000$ cm^{-3} and $R \lesssim 1.1$ kpc) might not apply if the ionization changes occurred out of equilibrium. In particular, ionization *increases* caused by a rise in the ionizing flux could occur much faster than the recombination time. The most likely explanation for the line changes between 2006.64 and 2008.67 is, indeed, an ionization increase (Section 4.3 below). However, there is weak evidence for both weakening and strengthening of the C IV lines in J2123 $-$ 0050 (Fig. 3), which is typical variable outflow lines in quasars (Hamann et al. 1995, 1997a; Narayanan et al. 2004; Misawa et al. 2007b; Capellupo et al. 2010; Gibson et al. 2010; Rodríguez Hidalgo et al., in preparation). If this up-and-down behaviour of the line strengths represents changes in the ionization (see also Misawa et al. 2007b), then recombination must be involved. Continued high-resolution monitoring is needed to confirm that conclusion specifically for J2123 $-$ 0050. However, even if the line variations in this object occurred because of clouds crossing our view of the continuum source, basic assumptions about the crossing speeds would require a radial distance much smaller than the 1.1-kpc limit derived from the recombination time (Section 4.3). Therefore, we adopt $R \lesssim 1.1$ kpc as a firm upper limit.

3.7 Metal abundances

We estimate the C/H metal abundance from the average measured ratio of $N(\text{C IV})/N(\text{H I}) \sim 2.5$ in system C (Tables 3 and 4) and an ionization correction based on $\log U \sim -0.4$ (see equation A2 and Fig. A1). This indicates [C/H] $\sim$0.3 $\pm$ 0.2, where the square brackets have their usual meaning of log abundance relative to solar and the 1σ uncertainty includes an estimate of the errors in both the column densities and the ionization correction. The uncertainties related to the ionization are small because the most likely ionization parameter, $\log U \sim -0.4$, is near the peak in the C IV ion fraction curve where the correction factor, $f(\text{H I})/f(\text{C IV})$, is not sensitive to the specific value of $\log U$ across a fairly wide range. A careful inspection of the numerical results depicted in Fig. A1 shows that $f(\text{H I})/f(\text{C IV})$ stays constant within $\pm$0.1 dex across a range in $\log U$ from -1.4 to 0.0. Moreover, this range in $\log U$ encompasses the minimum value of $f(\text{H I})/f(\text{C IV})$ at $\log U = -0.75$ (Table A1). If we apply the minimum correction factor $\log[f(\text{H I})/f(\text{C IV})] = -3.80$ (Table A1) to the system C column densities, we derive a lower limit on the metal abundance, [C/H] $\gtrsim 0.2$, which is close to our best estimate above but completely independent of the ionization uncertainties (see also Hamann 1997).

4 DISCUSSION

Section 3 presented measurements and analysis of five distinct outflow NAL systems in J2123 $-$ 0050 having C IV linewidths of FWHM $\sim$ 62 to 164 km s^{-1} and velocity shifts from $v \sim -9710$ to $-14\,050$ km s^{-1} in the quasar rest frame. These systems appear to be physically related based on their roughly similar line strengths, kinematics, ionizations, line-of-sight covering factors and coordinated variabilities. They provide a wealth of information about a particular NAL outflow that is valuable for comparison to other work on BAL and mini-BAL outflows. Here we discuss some additional results and implications. Please see Section 5 below for an overall summary.

4.1 Location summary

The formation of the variable NALs in a quasar outflow is confirmed by all three properties of line variability, partial covering and resolved profiles that are smooth and broad compared to thermal linewidths. Moreover, if we accept that the lines form somewhere in the quasar environment based on these properties, then the only plausible location is a quasar-driven outflow because the velocity shifts are much too large to be explained by other near-quasar environments such as a galactic starburst-driven wind or a nearby galaxy in the same cluster as the quasar (Rupke, Veilleux & Sanders 2005; Prochaska & Hennawi 2009). By matching the variability to a recombination time, we place an upper limit on the distance between the absorber and the quasar of $R \lesssim 1.1$ kpc (Section 3.6). At the opposite extreme, constraints on the acceleration suggest that the NAL gas is coasting freely at a distance $R \gtrsim 5$ pc (Section 3.5). Thus the full range of plausible distances is $5 \lesssim R \lesssim 1100$ pc. However, if the absorbing structures are small blobs or filaments created in the inner flow, their most likely location is near the ~ 5 pc minimum radius because such structures will travel just a few pc before dissipating (if there is no external confinement; Section 4.4 below).

Finally, our estimate of the metallicity, [C/H] $\sim 0.3 \pm 0.2$ with a lower limit of [C/H] $\gtrsim 0.2$, is also consistent with the formation of these NALs in a quasar outflow. Supersolar metallicities are extremely rare in intervening absorption line systems, having been observed so far only in a few Lyman-limit and super-Lyman-limit systems (Prochaska et al. 2006; Prochter et al. 2010), but they are typical of near-quasar environments based on estimates from the broad emission lines (Hamann & Ferland 1999; Dietrich et al. 2003; Nagao, Marconi & Maiolino 2006) and from other well-studied cases of NAL outflows (D'Odorico et al. 2004; Gabel et al. 2005, 2006; Arav et al. 2007, ; Simon, Hamann & Pettini, in preparation).

4.2 The outflow origins of quasar NALs

It is interesting to note that the outflow NALs in J2123 − 0050 are unresolved and indistinguishable from cosmologically intervening lines in medium-resolution spectra like the SDSS. They are much too narrow to be identified with an outflow using one of the absorption line indices designed for this purpose (Weymann et al. 1991; Trump et al. 2006). Their velocity shifts are also well above the nominal $|v| < 5000$ km s^{-1} cut-off used to define 'associated' absorption lines (AALs), which are likely to have a physical relationship to the quasar based on their statistical excess at $z_a \approx z_e$ compared to $z_a \ll z_e$ (Weymann et al. 1979; Foltz et al. 1986; Nestor et al. 2008; Wild et al. 2008). Without high-resolution spectra or multi-epoch observations to test for variability, the outflow NALs in J2123 − 0050 would be mistakenly attributed to cosmologically intervening gas.

The outflow systems are, in fact, surrounded in the J2123 − 0050 spectrum by other narrow C IV lines that did not vary, do not have partial covering and almost certainly do form in unrelated intervening material (Fig. 1). One of these intervening systems is at a smaller velocity shift than the outflow lines (at $v \sim 6987$ km s^{-1}), while another is blended directly with the outflow system E (see also Table 2 and Fig. 5). This mixture of lines in the same spectrum clearly demonstrates that velocity shift alone is a poor indicator of the outflow versus intervening origin of narrow absorption lines (see also Simon & Hamann 2010).

The secure outflow origin of the NALs in J2123 − 0050 lends anecdotal support to recent claims that a significant fraction of narrow C IV systems, even at large velocity shifts, form in quasar outflows. For example, Richards (2001) argued that ~ 36 per cent of high-velocity NALs originate in outflows based on a correlation between the numbers of these systems detected and the radio properties of the background quasars. Misawa et al. (2007a) estimated that 10–17 per cent of narrow high-velocity C IV systems belong to quasar outflows based on the incidence of partial covering measured in high-resolution spectra. Similar results were obtained more recently by Simon et al. (in preparation). Nestor et al. (2008) showed that the statistical excess of C IV NALs near the quasar redshift extends out to at least $\sim 12\,000$ km s^{-1}, e.g. well beyond the nominal cut-off of 5000 km s^{-1} for 'associated' absorption lines. They argue that $\gtrsim 43$ per cent of NALs stronger than REW = 0.3 Å in the velocity range $750 \lesssim v \lesssim 12\,000$ km s^{-1} originate in quasar outflows (also Wild et al. 2008). In their analysis of mostly weaker systems, Simon et al. (in preparation) find that roughly 20–25 per cent of C IV NALs in this velocity range exhibit partial covering.

The variable lines in J2123 − 0050 are unique in that they are (so far) the highest velocity NALs known to originate in a quasar outflow based on all three indicators of line variability, partial covering and superthermal linewidths. Their closest analogues in the literature are a complex of NALs at somewhat lower speeds, $v \sim 9500$ km s^{-1}, in the redshift 2.5 quasar HS 1603+3820 (Misawa et al. 2005, 2007b), and an isolated broader (FWHM ~ 400 km s^{-1}) outflow system at $v \sim 24\,000$ km s^{-1} in the $z_e \approx 2.5$ quasar Q2343+125 (Hamann, Barlow & Junkkarinen 1997c).

4.3 What caused the NAL variability?

The key properties of the NAL variability in J2123 − 0050 are (1) the line variations were well coordinated between the five systems, each with larger changes in C IV than O VI, (2) changes in the NAL strengths were accompanied by roughly commensurate changes in the line of sight covering fractions and (3) the variability time is ≤ 0.63 yr in the quasar rest frame.

Changes in the covering fractions would seem to have a natural explanation in clouds moving across our lines of sight to the background emission source. This explanation is, in fact, favoured by some recent studies of BAL variability (Gibson et al. 2008, 2010; Hamann et al. 2008; Capellupo et al. 2010). However, in J2123 − 0050, line changes induced by crossing clouds appear unlikely because the coordinated variations in five distinct NAL systems would require highly coordinated movements between five distinct absorbing structures in the outflow (also Misawa et al. 2005). Moreover, crossing clouds would need to traverse a significant fraction of the emission source diameter in ≤ 0.63 yr to cause the observed line variations. In Section 3.4 we argued that the relevant emission source is the accretion disc with diameter $D_{1550} \sim 0.026$ pc at 1550 Å. Crossing ≥ 15 per cent of that length in ≤ 0.63 yr, to explain the observed changes of order 0.15 in the C IV covering fractions, would require transverse speeds $v_{tr} \gtrsim 6000$ km s^{-1}. This seems unrealistic given that the radial flow speeds are not much larger, e.g. $v \sim -9710$ to 14 050 km s^{-1}. The maximum transverse speeds we might expect in a quasar outflow launched from a rotating accretion disc are of the order of the virial speed at the absorber location. A virial speed consistent with $v_{tr} \gtrsim 6000$ km s^{-1} in J2123 − 0050 would require that the absorber resides at a radial distance $\lesssim 2.4$ pc from the SMBH. This would place the absorbers inside of the minimum radius of 5 pc estimated above from the lack of radial acceleration (Section 3.5). It would also contradict the evidence from line-locking that the flow we observe is traveling primarily in a radial direction (Section 3.5).

A more likely explanation for the coordinated line variations is global changes in the ionization caused by fluctuations in the quasar's continuum flux. This situation could produce the observed changes in the covering fractions (Section 3.3) if the absorbers are spatially inhomogeneous, i.e. with a distribution of column densities across the emission source, such that the projected areas with $\tau_v \gtrsim 1$ in a given line change with the ionization state of the gas (Hamann & Sabra 2004). The observed decrease in the C IV line strengths between 2006.64 and 2008.67, accompanied by smaller or negligible changes in O VI, are consistent with an overall increase in the ionization parameter if the starting point was near the peak in the O VI ion fraction. In particular, an ionization parameter initially near $\log U \sim -0.4$ in 2006.64 and then increasing by a few tenths of a dex by 2008.67 would cause a decline in the C IV line strengths and column densities consistent with the observations (Table 3), while the O VI remains nearly constant (see Fig. A1).

This scenario requires that the quasar's far-UV continuum flux changed by a factor of roughly 2 in ≤ 0.63 yr (rest). Little is known about the far-UV variability properties of luminous quasars. None the less, this type of continuum change seems plausible given that (1) near-UV flux variations as large as 30–40 per cent have been observed in other luminous quasars on time-scales of months (rest, Kaspi et al. 2007), and (2) flux changes in the far-UV could be much larger than the near-UV because shorter continuum wavelengths generally exhibit larger amplitude fluctuations (Krolik et al. 1991; Vanden Berk et al. 2004).

The recent SDSS stripe 82 survey shows specifically that the near-UV continuum variability of $J2123 - 0050$ is typical of luminous quasars (Schmidt et al. 2010). This survey includes roughly 60 epochs of imaging photometry collected over a ~ 7-yr period that overlaps with our spectroscopic observations. Examination of these data for $J2123 - 0050$ (kindly provided by Kasper Schmidt) shows continuum variations up to ~ 0.27 mag (or ~ 28 per cent) on observed time-scales of ~ 2 yr in the r band (~ 2000 Å rest). Moreover, the r-band flux increased by this amount between roughly 2005.8 and the last stripe 82 data points in 2008.0, which is consistent with an our conclusion that the ionization increased between the Keck and VLT observations in 2006.64 and 2008.67.

The main caveat to interpreting the NAL variabilities in terms far-UV flux changes is that there *might* have been a large NAL variation between 2006.64 (Keck) and 2006.71 (MMT), i.e. in just ~ 8 d in the quasar frame (Fig. 3). If this extreme short-term variability can be confirmed, it might be difficult to explain via factor of ~ 2 changes in the far-UV emission from the accretion disc (but see also Misawa et al. 2007b).

4.4 Outflow structure

The outflow NALs in $J2123 - 005$ require at least five distinct absorbing structures that have similar physical conditions (ionization, column densities, covering fractions, Sections 3.3 and 3.4) and roughly similar kinematics (lines dispersions and velocity shifts, Section 3.5). The partial covering evident in all five systems indicates that the absorbers are each characteristically smaller than the quasar's UV continuum source, e.g. ~ 0.01–0.02 pc across. All five absorbers must also be spatially inhomogeneous to explain the observed changes in the covering fractions if those changes are, indeed, caused by changes in the quasar's ionizing flux (Section 4.3).

The absorbing structures might be discrete blobs or filaments created by instabilities in the inner flow, perhaps resembling the clumpy structures seen in some numerical simulations of BAL winds (Proga & Kallman 2004). If this assessment is correct, then their most likely location is near the minimum radius of $R \sim 5$ pc inferred from the lack of acceleration (Section 3.5). This is because small blobs or filaments have short survival times against dissipation if there is no external pressure confinement. The characteristic absorber diameter of $d \sim 0.015$ pc (Section 3.4) combined with the doppler parameters $b \sim 70$ km s^{-1} of the broader systems D and E (Table 3) indicate dissipation times of order $t_{\text{dis}} \sim d/b \approx 210$ yr. This is much longer than our observation timeline (Table 1) and therefore not a factor in the line variability. However, gas blobs moving radially at $v \sim 13\,500$ km s^{-1} (for systems D and E) will travel a distance of just ~ 3 pc before dissipating. Therefore, they should be located within ~ 3 pc of their point of origin. If that was the inner flow near the accretion disc (e.g. at radii not much greater than a few times $R_{\text{BELR}} \sim 0.65$ pc, Section 2.1, Murray & Chiang 1997; Proga, Stone & Kallman 2000), then the absorbers should reside near the $R \sim 5$ pc minimum radius (Section 4.1).

One puzzling constraint on the internal structure of these absorbers comes from the high densities. At $R \sim 5$ pc, the densities need to be near the upper end of the estimated range, $10^8 \gtrsim n_H \gtrsim 5000$ cm^{-3}, to avoid overionization by the intense quasar radiation field (Section 3.6). However, this entire density range is much larger than the average gas density, $\langle n_H \rangle \sim 215$ cm^{-3}, expected for absorbing clouds with total column density $N_H \sim 10^{19}$ cm^{-2} (Section 3.6) and characteristic size ~ 0.015 pc. This disparity implies that each of the five absorbers is composed of dense sheets or substructures that have radial thickness much smaller than their characteristic *transverse* size of ~ 0.015 pc. The combined radial thickness of these sheets or substructures in each absorbing region is just $N_H/n_H \sim 10^{11}$ cm if they are at $R \sim 5$ pc, or $\sim 2 \times 10^{15}$ cm at $R \sim 1100$ pc.

Some early studies of BALs presented similar arguments for the existence of dense substructures with an overall small volume filling factor in quasar outflows (Weymann, Turnshek & Christiansen 1985; Turnshek 1995). Those studies also recognized that the creation and survival of such small substructures present a serious theoretical challenge for outflow models (de Kool 1997). These concerns about substructure effectively ended when Murray et al. (1995) and Murray & Chiang (1997) proposed an attractive alternative, namely, that the flows could be spatially smooth and continuous if there is a shielding medium at the base of the flow that blocks most of the quasar's intense X-ray and far-UV radiation. With this shielding medium in place, the outflow gas behind the shield should be able to maintain the observed moderate degrees of ionization at much lower gas densities, thus allowing the flow to have an overall smooth spatial distribution. Subsequent X-ray observations supported this scenario by showing that BAL quasars are heavily absorbed in X-rays (Green & Mathur 1996; Mathur et al. 2000; Gallagher et al. 2002, 2006).

However, $J2123 - 0050$, like other NAL and mini-BAL outflow quasars, does not have strong X-ray absorption (Sections 1 and 2.2) and therefore it does not have a significant X-ray/far-UV shield (see also the calculations in Hamann & Simon 2010). Small dense substructures do appear necessary to explain the moderate degree of ionization at the inferred flow locations. Thus the debate about the existence of small substructures in quasar outflows remains open. These substructures might resemble the small-scale clumps identified recently in one detailed observational study of partial covering in a BAL outflow (Hall et al. 2007).

4.5 Acceleration and radiative shielding: comparisons to BAL outflows

The most remarkable aspect of the NAL outflow in J2123 − 0050 is the degree to which it contrasts with BAL flows. For example, it has high speeds and ionizations very similar to BALs, but the NALs we measure are about a hundred times narrower and a hundred times weaker (in REW) than typical BALs (cf. Table 2 and Weymann et al. 1991; Korista et al. 1993). Our estimate of the total column density, $N_H \sim 5 \times 10^{19}$ cm^{-2}, is also 1–2 orders of magnitude less than the best available estimates obtained from BALs (Hamann 1998; Arav et al. 2001; Hamann et al. 2002). The weak or absent X-ray absorption in J2123 − 0050 (Just et al. 2007) is typical of other NAL and mini-BAL outflow sources (Misawa et al. 2008; Chartas et al. 2009; Gibson et al. 2010), but it too is very different from the strong X-ray absorption found in BAL quasars (Mathur et al. 2000; Gallagher et al. 2002, 2006).

This disparity in the X-ray properties between BAL, mini-BAL and NAL outflows has important implications for outflow physics. As noted in Section 4.4, the prevailing models of radiatively driven BAL outflows have a shielding medium at the base of the flow that can absorb the quasar's ionizing far-UV/X-ray flux and thus prevent the overionization of the outflow gas behind the shield (Murray et al. 1995; Murray & Chiang 1997). Moderate ionizations in the outflow gas are essential to maintain significant opacities and facilitate the radiative acceleration to high speeds. However, the absence of strong X-ray absorption in J2123 − 0050 shows that high speeds and moderate ionizations can occur in quasar outflows *without* significant radiative shielding.

One way to reconcile these results is by a unified scheme where the outflows measured via BALs, NALs and mini-BALs coexist at different spatial locations. In situations like this (e.g. Ganguly et al. 2001; Chartas et al. 2009), the acceleration of the NAL and mini-BAL gas might occur in the shielded BAL environment (near the accretion disc plane) before it moves to its observed location (farther above the disc) where the shielding is negligible. The discrete appearance of NALs and mini-BALs in quasar spectra might be due to their formation in discrete blobs or filaments that are created via instabilities along the ragged edge of the main BAL outflow (Ganguly et al. 2001; Hamann et al. 2008). However, it is not clear there can be enough vertical force to push these blobs significantly away from the disc plane and out of their natural radial trajectories away from the UV continuum source. A more basic problem with this picture is that NALs and mini-BALs have degrees of ionization similar to BALs even though they are not behind the radiative shield that is alleged to be important for controlling the outflow ionization. If the NAL and mini-BAL gas is accelerated in a shielded BAL environment where it has moderate BAL-like ionizations, how does it maintain those moderate BAL-like ionizations after it emerges from the shielded BAL zone?

The obvious answer from our analysis of J2123 − 0050 (Sections 3.6 and 4.4) is that the outflow ionization is regulated mostly by locally high gas densities and not by a radiative shield. High densities could keep the ionization low enough for radiative acceleration even if there is no shielding at all. Perhaps this is the case generally in quasar outflows, including the BALs. However, high densities also lead to the uncomfortable conclusion that the outflows are composed of small substructures that have an overall small volume filling factor (Section 4.4). The physical processes that might create or maintain these substructures are not understood (de Kool 1997). None the less, the evidence for their existence in J2123 − 0050 is at least consistent with high densities playing a more important role in the acceleration physics than radiative shielding.

4.6 Energetics and feedback

Here we estimate the total mass and kinetic energy in the J2123 − 0050 outflow to determine if it can plausibly be important for feedback to the host galaxy's evolution (Section 1). If the flow geometry is approximately like part of a thin spherical shell, then its total mass is given by

$$M \approx 14 \left(\frac{Q}{10 \text{ per cent}} \right) \left(\frac{N_H}{5 \times 10^{19} \text{ cm}^{-2}} \right) \left(\frac{R}{5 \text{ pc}} \right)^2 \text{ M}_\odot, \quad (4)$$

where $N_H \approx 5 \times 10^{19}$ cm^{-2} is our best guess at the total column density in all five absorbing systems (Section 3.6), $R \approx 5$ pc is a likely radial distance (Sections 4.1 and 4.4) and Q is the global covering fraction of the outflow, i.e. the fraction of 4π steradians covered by the flow as seen from the central continuum source (Hamann 2000). The value of Q is not constrained by our data, but $Q \sim 10$ per cent is a reasonable guess based on estimates of the detection rates of high-velocity NAL outflows (Section 4.2). The outflow kinetic energy defined by $K = Mv^2/2$ is therefore

$$K \approx 2 \times 10^{52} \left(\frac{M}{14 \text{ M}_\odot} \right) \left(\frac{v}{12\,000 \text{ km s}^{-1}} \right)^2 \text{ erg}, \quad (5)$$

where $v \approx 12\,000$ km s^{-1} is roughly representative of all five systems.

To estimate the mass-loss rate and kinetic energy luminosity, we would need to make additional assumptions about the duration and radial structure of the flow (Hamann 2000). However, if we simply divide K from equation (5) by a characteristic flow time, $t_{\text{flow}} \sim R/v \sim 410$ yr (for $R \sim 5$ pc and $v \sim 12\,000$ km s^{-1}), we obtain a time-averaged kinetic luminosity of $\langle L_K \rangle \sim 2 \times 10^{42}$ erg s^{-1} and a ratio relative to the quasar's bolometric photon luminosity of only $\langle L_K \rangle / L \sim 2 \times 10^{-6}$ (Section 2.1). This estimate is much less than the ratio of $L_K/L \sim 5$ per cent expected if the outflow is to be important for feedback (Scannapieco & Oh 2004; Di Matteo et al. 2005; Prochaska & Hennawi 2009). We also note that the total kinetic energy given by equation (5) is equivalent to the non-neutrino output of only ~ 20 type II supernovae (at $K \sim 10^{51}$ erg each).

The total mass and kinetic energy could be much larger if the outflow gas is near the maximum radius, $R \sim 1100$ pc, derived in Section 3.6. In that case, equations (4) and (5) indicate $M \sim 7 \times 10^5$ M$_\odot$ and $K \sim 10^{57}$ erg, respectively. However, this value of K is still far less than the binding energy of gas in a massive galaxy ($\sim 10^{59}$–10^{60} erg), and the increased flow time at $R \sim 1100$ pc leads to a time-averaged kinetic energy yield, $\langle L_K \rangle / L \sim 4 \times 10^{-4}$, that is still 2 orders of magnitude below the fiducial mark of $L_K/L \sim 5$ per cent needed for feedback. Therefore, at any of the plausible absorber locations, the kinetic energy yield from this NAL outflow is much too small to be important for feedback to the host galaxy's evolution.

5 SUMMARY

We discuss multi-epoch spectroscopic observations of five outflow NAL systems in the luminous quasar J2123 − 0050. The lines have velocity shifts from −9710 to −14 050 km s^{-1} and C IV linewidths in the range FWHM ~ 62 to 164 km s^{-1} (as measured in 2006.64, Table 2). These are the highest-velocity NALs reported so far to have their formation in a quasar outflow confirmed by all three indicators

of line variability, partial covering of the quasar continuum source and smooth superthermal line profiles. The five distinct absorption line systems require five outflow structures with similar physical conditions, similar sizes (covering fractions) and roughly similar kinematics. All five systems have stronger absorption in O VI than C IV, while lower ions such as Si IV, C III and C II are significantly absent. The observed NAL variabilities were well coordinated between the five systems, with changes in the line strengths accompanied by nearly commensurate changes in the line of sight covering fractions. The time-scale for significant NAL changes is $\lesssim 0.63$ yr in the quasar rest frame. Our analysis of these data provides the following additional constraints on the outflow properties.

(1) *Absorbing region sizes.* Partial covering of the UV continuum source indicates that the C IV and O VI absorbing regions have characteristic sizes of order $\sim$0.01–0.02 pc (Section 3.4).

(2) *Ionization.* The absence of C III lines and stronger absorption in O VI compared to C IV in all five systems indicates an ionization parameter of $\log U \gtrsim -0.8$ (Section 3.6). The most likely value is near $\log U \sim -0.4$ based on the different variabilities observed in C IV and O VI (Section 4.3).

(3) *Variability.* The coordinated nature of the NAL variations occurring in $\lesssim 0.63$ yr is best explained by global ionization changes in the outflow caused by changes in the quasar's ionizing flux (Section 4.3). The magnitude of the ionization changes corresponds to roughly 0.2–0.3 dex in U.

(4) *Metallicity.* The secure detection of Lyα in one system indicates a metal abundance of [C/H] $\sim$0.3 $\pm$ 0.2, with a lower limit independent of ionization uncertainties of [C/H] $\gtrsim$ 0.2 (Section 3.7). These results are consistent with other estimates of quasar metallicities and they support the claim that the variable NALs in J2123 − 0050 form in a quasar outflow.

(5) *Total column density.* We estimate the total hydrogen column density in system C to be $N_{\mathrm{H}} \sim 10^{19}$ cm^{-2} based on $\log U \sim -0.4$ and the strength of Lyα in that system. From this and the many similarities between the variable systems, we infer that the total column density in all five systems is very roughly $N_{\mathrm{H}} \sim 5 \times 10^{19}$ cm^{-2} (Section 3.6).

(6) *Dynamics.* An upper limit on the radial acceleration, $\lesssim 3$ km s^{-1} yr^{-1}, and an apparent double line-lock in the C IV systems suggest that (i) the outflow was radiatively accelerated, (ii) it is now gravitationally unbound and coasting freely beyond the main acceleration zone and (iii) its trajectory is within $\sim 16°$ of the purely radial (line-of-sight) direction (Section 3.5).

(7) *Location.* The acceleration upper limit suggests that the outflow lines form in a low-gravity environment $\gtrsim 5$ pc from the central quasar (Section 3.5). The minimum gas density needed for recombination in $\lesssim 0.65$ yr sets an upper limit on the distance of $\sim$1100 pc (in photoionization equilibrium, Section 3.6). Thus the full range of plausible distances is $5 \lesssim R \lesssim 1100$ pc. If the absorbing structures are blobs or filaments created in the inner flow, their short survival times against dissipation (in the absence of a confining pressure) indicates that they are near the minimum radius of $\sim$5 pc (Section 4.4).

(8) *Density and substructure.* The gas densities corresponding to distances $5 \lesssim R \lesssim 1100$ pc are $10^8 \gtrsim n_{\mathrm{H}} \gtrsim 5000$ cm^{-3} for a gas in photoionization equilibrium at $\log U \gtrsim -0.8$ (Section 3.6). These densities are much larger than the average value $\langle n_{\mathrm{H}} \rangle \sim 215$ cm^{-3} expected from the total column density and characteristic size. Therefore, each of the five absorbers is composed of dense thin sheets or substructures with an overall small volume filling factor (Section 4.4).

(9) *Radiative shielding and acceleration.* The absence of strong X-ray absorption in J2123 − 0050 (Just et al. 2007) is typical of NAL and mini-BAL outflows but contrasts markedly with BAL quasars. It implies that radiative shielding in the X-ray/far-UV is not needed to keep the outflow ionizations moderate (and BAL-like) and therefore, perhaps, it is not needed to facilitate the radiative acceleration of the flow to high speeds. We argue that the ionization is controlled, instead, by locally high gas densities in small outflow substructures (Section 4.5).

(10) *Energetics and feedback.* At the most likely radial distance near $R \sim 5$ pc, this outflow has a total mass of only $\sim$14 M$_\odot$ and kinetic energy $\sim 2 \times 10^{52}$ erg. At any of the plausible larger distances noted above, the kinetic energy yield from this outflow is still at least 2 orders of magnitude too small to be important for feedback to the host galaxy's evolution (Section 4.6).

REFERENCES

Adelman-McCarthy J. K. et al., 2008, ApJS, 175, 297
Arav N. et al., 2001, ApJ, 561, 118
Arav N., Kaastra J., Kriss G. A., Korista K. T., Gabel J., Proga D., 2005, ApJ, 620, 665
Arav N. et al., 2007, ApJ, 658, 829
Arav N., Moe M., Costantini E., Korista K. T., Benn C., Ellison S., 2008, ApJ, 681, 954
Arnaud M., Rothenflug R., 1985, A&AS, 60, 425
Asplund M., Grevesse N., Sauval A. J., Scott P., 2009, ARA&A, 47, 481
Barlow T. A., Sargent W. L. W., 1997, AJ, 113, 136
Becker R. H., White R. L., Helfand D. J., 1995, ApJ, 450, 559
Bentz M. C., Denney K. D., Peterson B. M., Pogge R. W., 2007, in Ho L. C., Wang J.-W., eds, ASP Conf. Ser. Vol. 373, The Central Engine of Active Galactic Nuclei. Astron. Soc. Pac., San Francisco, p. 380
Braun E., Milgrom M., 1989, ApJ, 342, 100
Capellupo D., Hamann F. Rodríguez Hidalgo P., Shields J., 2010, MNRAS, submitted
Chartas G. et al., 2009, New Astron. Rev., 53, 128
D'Odorico V., Cristiani S., Romano D., Granato G. L., Danese L., 2004, MNRAS, 351, 976
de Kool M., 1997, in Arav N., Shlosman I., Weymann R. J., eds, ASP Conf. Ser. Vol. 128, Mass Ejection from Active Galactic Nuclei. Astron. Soc. Pac., San Francisco, p. 233
de Kool M., Korista K. T., Arav N., 2002, ApJ, 580, 54
Di Matteo T., Springel V., Hernquist L., 2005, Nat, 433, 604
Dietrich M., Hamann F., Shields J. C., Constantin A., Heidt J., Jäger K., Vestergaard M., Wagner S. J., 2003, ApJ, 589, 722

Elvis M. et al., 1994, ApJS, 95, 1

Everett J. E., 2005, ApJ, 631, 689

Farrah D., Lacy M., Priddey R., Borys C., Afonso J., 2007, ApJ, 662, L59

Ferland G. J., Korista K. T., Verner D. A., Ferguson J. W., Kingdon J. B., Verner E. M., 1998, PASP, 110, 761

Foltz C. B., Weymann R. J., Peterson B. M., Sun L., Malkan M. A., Chaffee F. H., Jr,, 1986, ApJ, 307, 504

Foltz C. B., Weymann R. J., Morris S. L., Turnshek D. A., 1987, ApJ, 317, 450

Gabel J. R. et al., 2005, ApJ, 623, 85

Gabel J. R., Arav N., Kim T.-S., 2006, ApJ, 646, 742

Gallagher S. C., Brandt W. N., Chartas G., Garmire G. P., 2002, ApJ, 567, 37

Gallagher S. C., Brandt W. N., Chartas G., Priddey R., Garmire G. P., Sambruna R. M., 2006, ApJ, 644, 709

Ganguly R., Brotherton M. S., 2008, ApJ, 672, 102

Ganguly R., Eracleous M., Charlton J. C., Churchill C. W., 1999, AJ, 117, 2594

Ganguly R., Bond N. A., Charlton J. C., Eracleous M., Brandt W. N., Churchill C. W., 2001, ApJ, 549, 133

Ganguly R., Masiero J., Charlton J. C., Sembach K. R., 2003, ApJ, 598, 922

Gaskell C. M., 2008, in Benítez E., Cruz-González I., Krongold Y., eds, Accretion Disks and the Nature and Origin of AGN Continuum Variability, Rev. Mex. Astron. Astrofis. Conf. Ser. Vol. 32. Instituto de Astronomía, México, p. 1

Gibson R. R., Brandt W. N., Schneider D. P., Gallagher S. C., 2008, ApJ, 675, 985

Gibson R. R. et al., 2009a, ApJ, 692, 758

Gibson R. R., Brandt W. N., Gallagher S. C., Schneider D. P., 2009b, ApJ, 696, 924

Gibson R. R., Brandt W. N., Gallagher S. C., Hewett P. C., Schneider D. P., 2010, ApJ, 713, 220

Granato G. L., De Zotti G., Silva L., Bressan A., Danese L., 2004, ApJ, 600, 580

Green P. J., Mathur S., 1996, ApJ, 462, 637

Hall P. B., Hutsemékers D., Anderson S. F., Brinkmann J., Fan X., Schneider D. P., York D. G., 2003, ApJ, 593, 189

Hall P. B., Sadavoy S. I., Hutsemekers D., Everett J. E., Rafiee A., 2007, ApJ, 665, 174

Hamann F., 1997, ApJS, 109, 279

Hamann F., 1998, ApJ, 500, 798

Hamann F., 2000, in Murdin P., ed., Encyclopedia of Astronomy and Astrophysics. Bristol Institute of Physics Publishing, Bristol

Hamann F., Ferland G., 1999, ARA&A, 37, 487

Hamann F., Sabra B., 2004, in Richards G. T., Hall P. B., eds, ASP Conf. Ser. Vol. 311, AGN Physics with the Sloan Digital Sky Survey. Astron. Soc. Pac., San Francisco, p. 203

Hamann F., Simon L. E., 2010, MNRAS, submitted

Hamann F., Korista K. T., Morris S. L., 1993, ApJ, 415, 541

Hamann F., Barlow T. A., Beaver E. A., Burbidge E. M., Cohen R. D., Junkkarinen V., Lyons R., 1995, ApJ, 443, 606

Hamann F., Barlow T., Cohen R. D., Junkkarinen V., Burbidge E. M., 1997a, in Arav N., Shlosman I., Weymann R. J., eds, ASP Conf. Ser. Vol. 128, Mass Ejection from Active Galactic Nuclei. Astron. Soc. Pac., San Francisco, p. 19

Hamann F., Barlow T. A., Junkkarinen V., Burbidge E. M., 1997b, ApJ, 478, 80

Hamann F., Barlow T. A., Junkkarinen V., 1997c, ApJ, 478, 87

Hamann F. W., Barlow T. A., Chaffee F. C., Foltz C. B., Weymann R. J., 2001, ApJ, 550, 142

Hamann F., Korista K. T., Ferland G. J., Warner C., Baldwin J., 2002, ApJ, 564, 592

Hamann F., Kaplan K. F., Hidalgo P. R., Prochaska J. X., Herbert-Fort S., 2008, MNRAS, 391, L39

Häring N., Rix H., 2004, ApJ, 604, L89

Herbert-Fort S., Prochaska J. X., Dessauges-Zavadsky M., Ellison S. L., Howk J. C., Wolfe A. M., Prochter G. E., 2006, PASP, 118, 1077

Hewett P. C., Wild V., 2010, MNRAS, 405, 2302

Hopkins P. F., Elvis M., 2010, MNRAS, 401, 7

Hopkins P. F., Richards G. T., Hernquist L., 2007, ApJ, 654, 731

Just D. W., Brandt W. N., Shemmer O., Steffen A. T., Schneider D. P., Chartas G., Garmire G. P., 2007, ApJ, 665, 1004

Kaplan K. F. et al., 2010, PASP, in press

Kaspi S., Brandt W. N., Maoz D., Netzer H., Schneider D. P., Shemmer O., 2007, ApJ, 659, 997

Kauffmann G., Haehnelt M., 2000, MNRAS, 311, 576

Korista K. T., Voit G. M., Morris S. L., Weymann R. J., 1993, ApJS, 88, 357

Krolik J. H., Horne K., Kallman T. R., Malkan M. A., Edelson R. A., Kriss G. A., 1991, ApJ, 371, 541

Leighly K. M., Hamann F., Casebeer D. A., Grupe D., 2009, ApJ, 701, 176

Malec A. L. et al., 2010, MNRAS, 403, 1541

Marconi A., Hunt L. K., 2003, ApJ, 589, L21

Mathur S. et al., 2000, ApJ, 533, L79

Misawa T., Eracleous M., Charlton J. C., Tajitsu A., 2005, ApJ, 629, 115

Misawa T., Charlton J. C., Eracleous M., Ganguly R., Tytler D., Kirkman D., Suzuki N., Lubin D., 2007a, ApJS, 171, 1

Misawa T., Eracleous M., Charlton J. C., Kashikawa N., 2007b, ApJ, 660, 152

Misawa T., Eracleous M., Chartas G., Charlton J. C., 2008, ApJ, 677, 863

Murray N., Chiang J., 1997, ApJ, 474, 91

Murray N., Chiang J., Grossman S. A., Voit G. M., 1995, ApJ, 451, 498

Nagao T., Marconi A., Maiolino R., 2006, A&A, 447, 157

Narayanan D., Hamann F., Barlow T., Burbidge E. M., Cohen R. D., Junkkarinen V., Lyons R., 2004, ApJ, 601, 715

Nestor D., Hamann F., Rodriguez Hidalgo P., 2008, MNRAS, 386, 2055

Netzer H., Lira P., Trakhtenbrot B., Shemmer O., Cury I., 2007, ApJ, 671, 1256

Peterson B. M., 1997, An Introduction to Active Galactic Nuclei. Cambridge Univ. Press, Cambridge

Prochaska J. X., Hennawi J. F., 2009, ApJ, 690, 1558

Prochaska J. X., O'Meara J. M., Herbert-Fort S., Burles S., Prochter G. E., Bernstein R. A., 2006, ApJ, 648, L97

Prochter G. E., Prochaska J. X., O'Meara J. M., Burles S., Bernstein R. A., 2010, ApJ, 708, 1221

Proga D., Kallman T. R., 2004, ApJ, 616, 688

Proga D., Stone J. M., Kallman T. R., 2000, ApJ, 543, 686

Richards G. T., 2001, ApJS, 133, 53

Richards G. T. et al., 2006, ApJS, 166, 470

Rupke D. S., Veilleux S., Sanders D. B., 2005, ApJS, 160, 115

Savage B. D., Sembach K. R., 1991, ApJ, 379, 245

Scannapieco E., Oh S. P., 2004, ApJ, 608, 62

Schmidt K. B., Marshall P. J., Rix H., Jester S., Hennawi J. F., Dobler G., 2010, ApJ, 714, 1194

Shemmer O., Netzer H., Maiolino R., Oliva E., Croom S., Corbett E., di Fabrizio L., 2004, ApJ, 614, 547

Shen Y. et al., 2007, AJ, 133, 2222

Simon L. E., Hamann F., 2010, MNRAS, submitted

Srianand R., Petitjean P., 2000, A&A, 357, 414

Srianand R., Petitjean P., Ledoux C., Hazard C., 2002, MNRAS, 336, 753

Steffen A. T., Strateva I., Brandt W. N., Alexander D. M., Koekemoer A. M., Lehmer B. D., Schneider D. P., Vignali C., 2006, AJ, 131, 2826

Strateva I. V., Brandt W. N., Schneider D. P., Vanden Berk D. G., Vignali C., 2005, AJ, 130, 387

Telfer R. C., Zheng W., Kriss G. A., Davidsen A. F., 2002, ApJ, 565, 773

Tremaine S. et al., 2002, ApJ, 574, 740

Trump J. R. et al., 2006, ApJS, 165, 1

Turnshek D. A., 1995, in Meylan G., ed., Proc. ESO Workshop, QSO Absorption Lines The Covering Factors, Ionization Structure, and Chemical Composition of QSO Broad Absorption Line Region Gas. Springer, Berlin, p. 223

Tytler D., Fan X.-M., 1992, ApJS, 79, 1

Vanden Berk D. E. et al., 2004, ApJ, 601, 692

Verner D. A., Verner E. M., Ferland G. J., 1996, Atomic Data and Nuclear Data Tables, 64, 1

Vestergaard M., Peterson B. M., 2006, ApJ, 641, 689

Warner C., Hamann F., Dietrich M., 2004, ApJ, 608, 136

Weymann R. J., Williams R. E., Peterson B. M., Turnshek D. A., 1979, ApJ, 234, 33

Weymann R. J., Turnshek D. A., Christiansen W. A., 1985, in Miller J. S., ed., Astrophysics of Active Galaxies and Quasi-Stellar Objects, Broad Absorption Line Quasars ('BALQSOs'), University Science Books, Mill Valley, CA, p. 333

Weymann R. J., Morris S. L., Foltz C. B., Hewett P. C., 1991, ApJ, 373, 23

Wild V. et al., 2008, MNRAS, 388, 227

APPENDIX A: PHOTOIONIZATION CALCULATIONS

We use the numerical code CLOUDY, version 08.00 (last described by Ferland et al. 1998), to compute ionization fractions for clouds that are in photoionization equilibrium with a quasar continuum source. The results have wide applicability to quasar outflows and a variety of other near-quasar environments. The calculations assume that the gas clouds are dust free, at a constant density throughout, optically thin in the Lyman continuum and geometrically thin such that their radial thickness, ΔR, is small compared to their distance, R, from the ionizing emission source, i.e. $\Delta R/R \ll 1$. The optically thin assumption ensures that the model clouds have a uniform ionization structure throughout. This is appropriate for the majority of quasar outflow systems, including J2123−0050, that are highly ionized with $N(\mathrm{H\,I}) \lesssim 10^{17.2}$ cm^{-2}. (Moderate continuum opacities can occur at the He II ionization edge for $10^{16.5} \lesssim N(\mathrm{H\,I}) \lesssim 10^{17.2}$ cm^{-2}, but this has no significant affect on the ionization fractions discussed here; Hamann 1997) The calculations assume that the metallicity is solar and the total hydrogen density is $n_{\mathrm{H}} = 10^5$ cm^{-3}, although the specific values of these parameters do not affect the ionization results (Hamann 1997).

The quasar spectrum is a simple segmented power law consistent with observational constraints across the most important far-UV energies (Elvis et al. 1994; Telfer et al. 2002; Richards et al. 2006; Steffen et al. 2006; Hopkins, Richards & Hernquist 2007, and references therein). It has the form $f_\nu \propto \nu^\alpha$ with slope $\alpha = -1.0$ from 0.5 to 13.6 eV, $\alpha = -2.56$ from 13.6 to 136 eV, and $\alpha = -1.0$ from 136 to 136 keV. Sharper cut-offs are applied to the high- and low-energy extremes ($\alpha = 3$ below 0.5 eV and $\alpha = -3$ above 136 keV) that have no effect on the computed ionizations. This spectrum yields $\alpha_{\mathrm{ox}} = -1.6$ (appropriate for luminous radio-quiet quasars; Strateva et al. 2005; Steffen et al. 2006), and a bolometric correction factor at 1450 Å of $L \approx 4.4\,\nu L_\nu(1450\,\text{Å};)$ (see also Warner et al. 2004).

We describe the ionization state of the gas in terms of the dimensionless ionization parameter, $U \equiv \Phi_{\mathrm{H}}/(4\pi c\, n_{\mathrm{H}} R^2)$, where Φ_{H} is the hydrogen-ionizing photon luminosity of the central source (Ferland et al. 1998). For the continuum shape described above, this yields the following expression for the radial distance

$$R = 225 \left(\frac{\nu L_\nu(1450\,\text{Å})}{10^{47}\,\mathrm{erg\,s^{-1}}} \right)^{1/2} \left(\frac{10^5\,\mathrm{cm^{-3}}}{n_{\mathrm{H}}} \right)^{1/2} \left(\frac{0.1}{U} \right)^{1/2} \mathrm{pc}. \quad \text{(A1)}$$

Fig. A1 shows the calculated ionization fractions for H I and several metal ions commonly observed in near-UV spectra of quasars, namely, ions of C, N, O and Si. One important application of these results to absorption line work is derivations of metal-to-hydrogen (M/H) abundance ratios based on this relation:

$$\left[\frac{\mathrm{M}}{\mathrm{H}} \right] = \log \left(\frac{N(\mathrm{M}_i)}{N(\mathrm{H\,I})} \right) + \log \left(\frac{f(\mathrm{H\,I})}{f(\mathrm{M}_i)} \right) + \log \left(\frac{\mathrm{H}}{\mathrm{M}} \right)_\odot, \quad \text{(A2)}$$

where $(\mathrm{H/M})_\odot$ is the solar abundance ratio by number, and N and f are the column densities and ionization fractions, respectively, for H I and the metal M in ion stage i. Ideally, one would apply equation (2) after comparing the measured column densities in several metal ions to the calculated results (Fig. A1) in order to define U and an appropriate ionization correction factor, $f(\mathrm{H\,I})/f(\mathrm{M}_i)$.
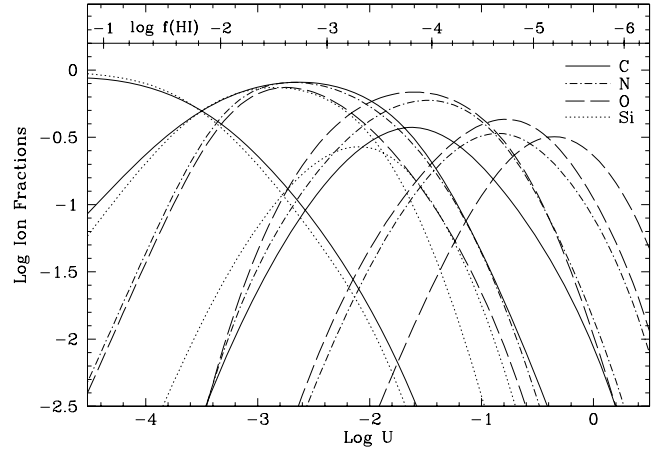
Figure A1. Ion fractions, $f(\mathrm{M}_i)$, for selected stages of the elements C, N, O and Si plotted against the ionization parameter, $\log U$, in optically thin photoionized clouds (see text). From left to right the three curves plotted for carbon are for C II, C III and C IV. The remaining curves (left to right) are for nitrogen: N III, N IV and N V, oxygen: O III, O IV, O V and O VI, and silicon: Si II, Si III and Si IV. The H I fraction, $\log f(\mathrm{H\,I})$, at each $\log U$ is marked along the horizontal bar near the top.

Table A1. Minimum ionization corrections.

Element	II	III	IV	V	VI
	Minimum $\log[f(\mathrm{H\,I})/f(\mathrm{M}_i)]$				
Carbon	−1.75	−3.32	−3.80	−5.39	—
Nitrogen	−1.75	−3.28	−4.15	−4.55	−5.89
Oxygen	−1.81	−3.02	−4.17	−4.69	−5.06
Aluminium	−2.12	−2.20	−3.36	−4.11	−4.96
Silicon	−1.65	−2.93	−3.03	−3.89	−4.51
Phosphorus	−1.90	−3.10	−3.34	−3.57	−4.42
Sulfur	−1.50	−2.95	−3.73	−3.73	−3.97
	$\log U$ at minimum $\log[f(\mathrm{H\,I})/f(\mathrm{M}_i)]$				
Carbon	−2.60	−1.55	−0.75	0.30	—
Nitrogen	−3.20	−1.50	−0.75	−0.15	0.65
Oxygen	−3.15	−1.65	−0.75	−0.15	0.30
Aluminium	−2.60	−2.10	−1.50	−0.70	−0.10
Silicon	−2.80	−1.95	−1.55	−1.00	−0.35
Phosphorus	−2.60	−1.80	−1.35	−1.00	−0.50
Sulfur	−2.90	−1.65	−1.20	−0.85	−0.60

However, if ionization constraints from the data are not available or not reliable, one can also use minimum values of the ionization corrections in equation (A2) to derive firm lower limits on the metal-to-hydrogen abundance ratios (Hamann 1997; Hamann & Ferland 1999).

Table A1 lists the minimum correction factors for various metal ions, $\log[f(\mathrm{H\,I})/f(\mathrm{M}_i)]$, together with the values of the ionization parameter, $\log U$, where these minima occur. This information is provided in the table according to the element (column 1) and ionization stage II–VI (columns 2–6) for ions that are sometimes detected in quasar outflow spectra. Note that the minimum correction factors occur near, but at larger U than, the peaks in the $f(\mathrm{M}_i)$ curves shown in Fig. A1. For convenience, we note that the most recent solar abundance ratios are $\log(\mathrm{H/M})_\odot = 3.57$ for carbon, 4.17 for nitrogen, 3.31 for oxygen, 5.55 for aluminium, 4.49 for silicon, 6.59 for phosphorus and 4.88 for sulfur (Asplund et al. 2009).